Construction and Building Materials 426 (2024) 136006

Contents lists available at ScienceDirect

Construction and Building Materials

journal homepage: www.elsevier.com/locate/conbuildmat

Microscopic analyses and performance characteristics of granite powder blended cement

P. Jagadesh [a,*], Solomon Oyebisi [b,c], A. Hareesh Muthu [a], A. Sarulatha [a], K. Supikshaa [a], V.P. Vhishva laxmy [a]

[a] Department of Civil Engineering, Coimbatore Institute of Technology, Coimbatore, Tamil Nadu 641 014, India
[b] Department of Civil Engineering, The University of the South Pacific, Suva, Fiji
[c] Department of Civil Engineering, Covenant University, PMB Ota 1023, Nigeria

ARTICLE INFO

Keywords:
Cement
Characterizations
Compressive strength
Granite powder
Lifecycle assessment
Modelling
Sustainability

ABSTRACT

This research investigates the characteristics of Granite Powder (GrP) and its potential use as a partial replacement for cement in mortar production. The GrP samples were analyzed via microscopic techniques. The effects of GrP Blended Cement (GrPBC) were examined on the workability and mechanical characteristics by partially replacing Ordinary Portland Cement (OPC) with 0–40 wt% GrP in 4 wt% increments. Life cycled assessment in terms of Embodied Energy (EE) and Global Warming Potential (GWP) of GrPBC-based mortar were assessed based on cradle-to-gate boundaries and the sustainability and economic indexes were determined at 28 days compressive strength. The study proposed new models to predict the compressive strength of GrPBC with respect to Water to Binder (W/B) ratio. The presence of active minerals depicts GrP as pozzolanic materials. The optimum replacement level of GrP in the blended mix, based on the fresh and hardened properties of GrPBC, is 20 wt% to achieve 75% of the strength activity index. GWP and EE declined as the GrP in the mixtures rose. The best sustainable and economic prospects were attained at the 25 wt% GrP replacement level. The compressive strength and the W/B ratio are highly correlated. Thus, GrP has proven to be a sustainable construction material in the construction sector.

1. Introduction

Concrete is the most widely used building material in the world, being employed in more than 70% of construction projects. Globally, about 25 billion tons of concrete are produced annually [1]. However, the manufacture of cement, a crucial component of concrete, is a major contributor to greenhouse gas emissions, the depletion of natural resources, and increased energy demand, all of which are causing climate change [2]. As such, the search for sustainable and alternative materials to replace cement in the manufacturing of concrete is imperative. Granite is one of the primary igneous rock types that is frequently utilized as a building material in construction. Minerals including feldspar, mica, and quartz are found in granite, which adds to its strength and durability [3]. India is the third biggest country of granite production in the globe after China and Brazil [4]. India contributes 46% of the global market for granite exports [5]. By exporting granite, India contributes 5.39% of its overall exports to the trade-to-gross domestic product ratio [5]. On production of granite blocks, there is production of 30% amount by weight during cutting and polishing [6]. Granite processing industries produce a huge quantity of granite waste in the form of Granite Powder (GrP), which is a by-product of the cutting and polishing of granite stones [7] [8]. The indiscriminate disposal of the GrP is an environmental challenge, leading to health hazards for humans and ecosystems. Some of notable GrP pollution in the water, soil, and air (dust) lead to the cancer and pneumoconiosis for humans [9,10]. However, disposal of GrP to soil in some cases, correct the acidic pH of the soil and enhances the increased content of calcium, magnesium and potassium in the soil [9].

Kala [11] noted improved mechanical properties of concrete when Natural Fine Aggregate (NFA) was partially replaced by GrP. The mechanical and durability properties of concrete blended with 25% NFA by GrP performed significantly better than conventional concrete. Sirianni et al. [12] reported that the there is difference in the Particle Size Distribution (PSD) of GrP due to the manufacturing process, which leads to variation in the silica content. Vijayalakshmi et al. [13] evaluated the

---

[*] Corresponding author.
E-mail addresses: jaga.86@gmail.com (P. Jagadesh), sotech281.ola@gmail.com (S. Oyebisi), hareeshmuthu5@gmail.com (A.H. Muthu), saruanand2001@gmail.com (A. Sarulatha), supikshaakathiresan@gmail.com (K. Supikshaa), vhishvalaxmy07@gmail.com (V.P. Vhishva laxmy).

https://doi.org/10.1016/j.conbuildmat.2024.136006
Received 10 November 2023; Received in revised form 13 February 2024; Accepted 25 March 2024

Nomenclature

GrP	Granite Powder
XRD	X-Ray Diffraction spectroscopy
FESEM	Field Emission Scanning Electron Microscope
EDS	Energy Dispersive Spectroscopy
EE	Embodied Energy
GWP	Global Warming Potential
RS	Raman Spectroscopy
FTIR	Fourier Transform Infra-Red Spectroscopy
XRF	X Ray Fluorescence spectrometer
OPC	Ordinary Portland Cement
GrPBC	Granite Powder Blended Cements
SCM	Supplementary Cementitious Materials
PSD	Particle Size Distribution
LCA	Life Cycle Assessment
TGA	Thermal Gravimetric Analysis
DSC	Differential Scanning Calorimetry
CSH	Calcium Silicate Hydrate
CH	Calcium Hydroxide
ICDD	International Centre for Diffraction Data
SAI	Strength Activity Index
SEM	Scanning Electron Microscope
ITZ	Interfacial Transition Zone
CASH	Calcium Aluminate Silicate Hydrate
W/B	Water to binder ratio

durability properties such as water permeability, rapid chloride penetration, carbonation depth, sulfate resistance and electrical resistivity of concrete made with GrP. Concrete made with partial replacement of NFA with GrP by 15% showed better mechanical and durability properties than the conventional concrete. Optimum percentage of partial replacement of NFA by GrP with satisfactory effect on the investigated parameters (fresh and hardened parameters) was found to be 25–40% [14,15]. Ghannam et al. [10] found that the partial replacement of NFA by GrP as 10% showed higher mechanical properties than the conventional concrete. The higher surface area of GrP showed higher bonding nature than that of NFA. Singh et al. [15] presented a review of earlier studies on substituting GrP with NFA. The results revealed that the GrP improved the mechanical and durability properties of concrete produced.

Prokopski et al. [16] reported an enhancement in the microstructural property of the GrP - based concrete. The use of GrP as a filler material in cementitious matrix systems increases the density and enhances the mechanical and durability qualities of concrete by having a significant positive impact on the filling pores [17]. Higher strength characteristics are found with an increase in density when NFA is replaced with GrP. In contrast, GrP contacts new products; hence, decreasing the pore volumes, but it does not isolate the new hydration phases or prevent the development of new products from hydration. Gupta and Vyas [18] reported enhancement of hardened properties of cementitious composites due to the GrP grains. Sadek et al. [19] investigated the impact of GrP on the fresh concrete mixes of self-compacting concrete (SCC). The results indicated that high volumes of the investigated GrP (up to 50% by weight of 400 kg/m^3 cement content) could be used successfully as mineral additives in the production of SCC. In general, SCC incorporating GrP showed the superior performance compared to the marble powder. Li et al. [20] reported the influence of plasticizer on the compressive strength of SCC produced with granite wastes. The water absorption of granite waste from the slurry resulted in increased hydration product of Magnesium hydroxide chlorides hydrates. The excess water absorption of granite waste from low-concentration brine led to compact microstructure of granite waste-fly ash-based blended cement, whereas from the high concentration of brine leads to porous microstructure.

Apart from the chemical compositions, PSD and surface texture are also important factors in determining the characterization of GrP and improving the hardened properties of concrete [21]. Materials engineering is the use of contemporary technologies to the functionalization of material powders (such as milling, sieving and grain surface) [22]. The effects of PSD of GrP on cement composites properties includes increased packing density, improved mixture uniformity, and increased compacting ability [22]. The specific surface area of the GrP grains influences the interaction of GrP with cementitious matrix systems and cement composites on the characteristics of hardened concrete [23,24]. The mechanical properties of the cement composite including GrP are generally improved by a larger specific surface area of GrP, which also improves the Interfacial Transition Zone (ITZ) between GrP grains and cement paste [25,26].

Karmegam et al. [27] reported that the addition of 10% GrP as partial replacement for the cement in SCC mixture resulted in improved compressive strength. Compressive strength was improved by roughly 9% for the concrete with 25% of NFA substituted by GrP as compared to the control concrete [28]. Ghannam et al. [10] found that partially replaced concrete of 20% NFA with GrP had a higher compressive strength than conventional concrete. Higher mechanical properties were attained because of GrP's greater specific surface area, which was produced with better cement hydration bonding. Better filler action of GrP and smaller particle size result in increased corrosion resistance of concrete containing GrP [29]. Ramos et al. [30] investigated the rapid chloride test on mortar containing GrP as a potential substitute for OPC. They found that 10% GrP in mortar led to a 70% increase in chloride resistance. Friedel's salt development (reaction of alumina content with GrP) and smaller particles are the cause of the rise in resistance. Using non-destructive evaluation studies, the introduction of new pozzolanic materials into concrete is assessed, and the improved hardened properties are documented in the literature [31,32]. The literature has reported that combining GrP with other wastes improves the characteristics of composites [33–36].

The literature reports on improving the characteristics of both fresh and hardened composites with GrP addition and determining the ideal GrP content [13,19]. Sadek et al. [19] reported pozzolanic and filler effect of the GrP on the cementitious composites. Refinement of pore structures due to presence of GrP enhances the hardened properties of GrP Blended Cement (GrPBC) [19]. Hence, there is a rising interest in the use of GrP as a partial replacement for the OPC in cement production [37,38]. The investigation of GrP characteristics and the performance of GrPBC is an area of research that has gained important attention in recent years.

Lifecycle assessment (LCA), as defined by ISO 14040 [39], is the process of gathering and evaluating a product system's inputs, outputs, and any environmental effects over the duration of its life [39]. The LCA, an internationally defined tool [39] for the comprehensive environmental assessment of products (GrPBC in this context), serves as the primary foundation for Lifecycle Thinking (LCT)'s environmental pillar. The LCT offers a useful tool for incorporating sustainability into product design, innovation, and assessment because of its systemic approach. There is evidence of this in several European institutions' policies [40–42] and international level [43,44] in which the core components are LCT and LCA. This is why this study proposes the LCA of GrPBC and its constituents, providing an informed decision regarding its environmental, societal, and economic impacts. According to earlier research, when recycled waste materials were blended with cement for concrete production, there was a decrease in global warming and embodied energy. Conversely, as the amount of recycled waste elements in concrete increased, so did its sustainability and economic potentials [45,46].

1.1. Novelty of the research

Analyzing the morphological characteristics, which will contribute to properties, is necessary to comprehend the behavior of GrP. Besides, additional research on the chemical compositions and chemical bonding of GrP is necessary to comprehend the performance of GrPBC. The role of GrP in the fresh and hardened properties of GrPBC can be better understood by first investigating the microscopic investigations of GrP. The techniques are X Ray Diffraction (XRD), Field Emission Scanning Electron Microscopy (FESEM), Energy Dispersive X-Ray Spectroscopy (EDS), Raman Spectroscopy (RS), Fourier Transform Infra-Red Spectroscopy (FTIR), Thermal analysis and X Ray Fluorescence spectroscopy (XRF). Furthermore, this study is original in that it assesses the lifecycle and sustainability of blended cement incorporating GrP. There is limited investigation on the optimal proportion of GrP that can be used as a partial replacement for OPC in cement production. It is necessary to evaluate the fresh and hardened properties of GrPBC. There are incomplete studies on the evaluation of modelling of the fresh and hardened properties of GrPBC. It is also necessary to evaluate the relationship between the water to binder (W/B) ratio and compressive strength of the GrPBC.

1.2. Objectives of the research

This study investigates the effects of GrP on blended cement using microscopic techniques such as XRD, FEMSEM, EDS, RS, FTIR, Thermal Analysis, and XRF. It evaluates the effects of GrP on the physical and mechanical properties of GrPBC. In addition, the research assesses the lifecycle of GrPBC using cradle-to-gate approach and evaluates the sustainability of the GrPBC blended mixes at 28 days of SAI. The models from literature are evaluated by determining the constants in the relationship while modelling the GrPBC water to binder ratio and compressive strength.

By fulfilling these objectives, the research will help create ecologically friendly and sustainable building materials that will lower the need for virgin raw materials, lessen the negative effects of construction waste on the environment, and enhance the functionality of cement-based materials. In addition, the findings will have positive consequences for reducing energy use, air and land pollution, and preserving natural resources.

2. Materials and methods

2.1. Materials

2.1.1. Granite powder

GrP was obtained from locally available granite stone quarry in the Local (Coimbatore) region, Tamil Nadu, India. GrP is a fine material, but it may still contain larger and smaller particles. Larger GrP particles were grinded in ball mill to reduce the particle size. Percentage of GrP retained in 45 μm was less than 10% and then the particles passing through 45 μm sieve was considered for use.

2.1.2. Ordinary Portland cement

The Ordinary Portland Cement (OPC) 53 grade cement according to IS 12269 [47] manufactured by Dalmia cements was used. A specific gravity test was conducted on the cement in accordance with Indian Standards and the result was 3.148. The OPC 53 Grade provides high strength to the structure because of its optimum PSD and superior crystallized structure [2]. However, it is important to note that OPC 53 grade cement has a higher heat of hydration than other types of cement, which can cause cracking if not properly managed.

2.2. Methods

2.2.1. Microscopic studies

Material characterization is the process of analyzing and identifying the properties of GrP to understand their behavior and performance. It is a crucial aspect of material science and engineering, as it provides important insights into the properties of GrP and their suitability for various applications.

2.2.1.1. X-ray diffraction (XRD) spectrometry. One of the common methods to study about the crystal structure of GrP is XRD spectroscopy. Empyrean, Malvern Panalytical instrument is used for powder sample in this study. GrP sample was mounted onto a glass slide using a small amount of adhesive. GrP was mounted to the glass slide in a manner that ensured the GrP was uniformly distributed and that there were no air bubbles between the GrP and the glass slide. GrP mounted on a glass slide was subsequently put into an X-ray diffractometer to analyze GrP. The GrP's crystal lattice diffracts X-rays that the diffractometer emits, creating a diffraction pattern that is indicative of the crystal structure of the sample. The sample's crystal structure and composition were determined by drawing the diffraction pattern using Origin Pro software and comparing it to data from the International Centre for Diffraction Data (ICDD).

2.2.1.2. Field scanning electron microscope (FESEM). With the aid of FESEM, GrP's morphological features were examined in order to comprehend its microstructural behavior. Caral Zeiss (Sigma) model of FESEM was used in this study to understand the morphological surface area. GrP with size less than 45 μm was used for this examination. Homogenous nature of GrP was maintained and the GrP particles were evenly distributed. To prevent GrP from charging, a gold conductive coating was placed to its surface using a sputter coater. An adhesive with a conductive characteristic was used to adhere GrP to carbon tape. During the FESEM analysis, the GrP sample was securely grasped. High-resolution images were generated by the interaction between the concentrated electron beam produced by the FESEM and the GrP. The images obtained from the FESEM analysis were analyzed to attain information about the morphology, size, and sample distribution.

2.2.1.3. Energy dispersive spectrometry (EDS). Bruker instrument attached to Zeiss model is used in this study for EDS to characterize GrP. EDS is a method used in combination with FESEM to analyze the chemical composition of material. In this study, gold was employed as a coating material on the GrP surface to prevent conductive material from charging. The GrP was coated using the sputtering technique. GrP was mounted onto a carbon tape via a conductive adhesive. It was ensured that the mounted GrP sample was stable throughout the investigation. Once the FESEM images were acquired, the EDS detector was used to collect X-ray spectra from the GrP. The detector measured the characteristic X-rays that were emitted by the elements in the GrP, providing information about their composition. The spectra obtained from EDS analysis were analyzed to identify the elements present in the GrP and their relative concentrations. Care was taken to avoid contaminating or damaging the sample during preparation and analysis.

2.2.1.4. Raman spectroscopy (RS). A small quantity of the grounded GrP was placed on a clean glass slide. Raman analyzer model of EZRaman N 532 was used in this investigation. The loose particles or debris around the GrP sample was removed using brush. The GrP sample was kept in the RS instrument by focusing the laser beam on the sample. Raman spectrum of the GrP was recorded with help of scanning the laser beam in the range of Raman wavelengths. Intensity of wavelength was recorded at various locations on the GrP. The chemical bonding of the GrP was identified using previously published Raman wavelengths from databases or literature.

2.2.1.5. Fourier transform infra-red (FTIR) spectrometry. FTIR is a technique used to analyze the chemical bonding nature of a sample based on the absorption of infrared radiation by the sample. Chemical bonding is analyzed with Bruker Model of Alpha series. Potassium bromide, an infrared transparent matrix material, was mixed with the powdered GrP sample to create a thin pellet. The composite pellet was prepared by placing a small quantity in the pellet press and pressing it at high pressure to form a thin, transparent disk. The composite pellet was placed inside the FTIR instrument, emitting infrared radiation and absorbing specific wavelengths of the radiation based on its chemical composition. A detector was used to measure the absorbed radiation, and the resulting spectra were recorded. The spectra obtained from FTIR analysis were analyzed to identify the functional groups present in the sample and their relative concentrations.

2.2.1.6. Thermal analysis. Thermal analysis is a method used to study the thermal performance of a material as a function of temperature. In this research, the thermal analysis of GrP was conducted using Thermogravimetric Analysis (TGA) using Netzsch analyzer and Differential Scanning Calorimetry (DSC) were measured by Mettler Toledo, DSC 822e. GrP was homogeneously maintained and processed to a fine powder. A small quantity of GrP was used and placed in the thermal instrument (DSC and TGA). The sample, as well as empty reference pan, were put in the thermal instrument, and the sample was heated at a specific heating rate. For the DSC, the GrP's heat flow was measured, and for the TGA, the GrP's weight loss was measured as a function of temperature. The phase transitions, melting point, and decomposition temperature of the GrP sample were estimated by analyzing the measured data.

2.2.1.7. X-ray fluorescence (XRF) spectrometry. XRF spectroscopy is a non-destructive analytical technique used to determine the elemental composition of material. Bruker model S8 Tiger and S4 Pioneer sequential wavelength is used for XRF analysis in this study. The coarser GrP was ground and sieved to achieve homogenization of the GrP. For the XRF analysis, the X-ray beam was applied to the GrP. Based on the chemical composition, which is identified by the sensor in the XRF instrument, GrP sample emits certain characteristics. Data obtained from GrP was analyzed with help of XRF to determine the chemical composition of the GrP.

2.2.2. Specific gravity of granite powder (GrP)

The specific gravity of GrP in this study was estimated using the displacement method, which includes measuring the weight of water evacuated by a known volume of the pozzolan [48]. The specific gravity of pozzolanic material is significant in estimating its density, which in turn affects its performance. The PSD of pozzolan is a significant factor that affects its reactivity, strength, and other physical properties [48]. Pozzolanic materials with a finer PSD generally exhibit higher reactivity and better pozzolanic properties, making them more suitable for use in various applications.

2.2.3. Granite powder blended cement (GrPBC) mixes

GrPBC mixes were proportioned by partially replacing OPC with 0–40 wt% GrP at 4 wt% increment. Different dosages of GrPBC samples were stored in the separate container in the sealed manner to prevent it from reacting with water. Table 1 displays the proportions of the mix design.

Table 1
Mix design proportions (kg/m^3).

% Replacement	OPC	GrP	Sand	Water
0	400	0	1200	109
4	384	16	1200	112
8	368	32	1200	116
12	352	48	1200	121
16	336	64	1200	126
20	320	80	1200	134
24	304	96	1200	144
28	288	112	1200	157
32	272	128	1200	173
36	256	144	1200	194
40	240	160	1200	220

2.2.3.1. Specific gravity. The specific gravity of GrPBC mixes were determined as per IS 4031–2 [49] using the standard Le Chatelier flask.

2.2.3.2. Consistency. The addition of water initiates the hydration process of GrPBC. One of the elements influencing the GrPBC's consistency is the GrPBC's fineness and chemical makeup. The standard consistency of the GrPBC blended cement paste was done according to the IS 4031–4 [50] with a standard Vicat apparatus conforming to IS 5513 [51] in a constant temperature of 27 °C and constant humidity of 90%. Water was added, starting at 25% and going up by 2% at a time, until the needle's penetration depth was between 5 and 7 mm from the bottom.

2.2.3.3. Setting times. The setting time decreases with faster cement hydration, which is influenced by the OPC and GrP's chemical makeup and fineness. The fresh and hardened properties of GrPBC paste are used to quantify the qualities of GrPBC. GrPBC's setting and hardening time is influenced by a number of factors, including temperature, humidity, and the type of GrP used. The initial and final setting time test of cement were determined as per IS 4031–5 [52] using a Vicat apparatus conforming to IS 5513 [51], balance of capacity 1 kg and sensitivity 1 g, and gauging trowel. The test was conducted at a temperature of 27 ± 2 °C and 65 ± 5% of relative humidity. A paste of 300 g of cement with 0.85 times the water required was prepared to give a paste of standard consistency [52]. In any case, the gauging process took no less than three minutes and no more than five minutes, and it was finished before any indication of setting appeared. The initial setting time was noted until the needle failed to penetrate the mold by 5 ± 0.5 mm. The final setting time was determined as the amount of time that passed between adding water to the GrPBC and the point at which the annular ring was unable to pierce the mould.

2.2.3.4. Strength activity index (SAI). GrPBC mortar was prepared with a proportion of GrPBC to standard sand in the ratio of 1:3. Quantity of water is arrived with help of consistency test. The compressive strength of GrPBC was performed at 7 and 28 days with the help of standard vibrating machine as per IS 4031–6 [53]. The water in which the cubes were submerged is replaced every 7 days, and the temperature is kept at 27 ± 2 °C. Average of three specimens was taken as compressive strength of GrPBC. Strength Activity Index (SAI), as illustrated in Eq. (1), is used to evaluate the strength gaining process of pozzolans at different ages [2]. The minimum SAI for natural pozzolan is 75% [54].

$$\mathrm{SAI}\ (\%) = \frac{A}{B} \times 100 \tag{1}$$

where A is the mean compressive strength of blended cement mortar cube and B is the mean compressive strength of control cement mortar cube.

2.2.4. Lifecycle assessments (LCA)

The four primary components of the LCA are used for the GrPBC: goal and scope, inventory analysis, impact assessment, and interpretation. The goal and scope were Embodied Energy (EE), Global Warming Potential (GWP), Sustainability Index (SI), and Economic Index (EI). Each mix, as contained in Table 1, is 1 m^3, which serves as the functional unit. The functional unit of GrPBC's GWP and EE are kgCO$_{2\text{-eq}}$/m^3 and MJ-eq/m^3, respectively. Moreover, the GrPBC's sustainability and economic indexes are set to ($kgCO_{2\text{-eq}}/m^3$)/MPa and (\$/m^3)/MPa functional units, respectively. The research focused only on the cradle-to-gate paradigm, encompassing all input and output flows from the limits of the cradle to the factory gate of the final processing operation [55]. The EE and GWP factors, as presented in Table 2, were obtained from the energy and carbon inventory [55]. The goal and scope were determined in accordance with the relationships illustrated in Eqs. (2)-(5) [45,46,55,56].

$$\mathrm{EE}(\text{cradle} - \text{to} - \text{gate}) = (1.22)\sum_{i=1}^{n}\left(m_w \times \mathrm{EE}_f\right) \tag{2}$$

$$\mathrm{GWP}(\text{cradle} - \text{to} - \text{gate}) = (1.19)\sum_{i=1}^{n}\left(m_w \times \mathrm{GWP}_f\right) \tag{3}$$

$$\mathrm{SI} = \frac{\mathrm{GWP} + (0.050 \times \mathrm{EE})}{28 - \text{day compressive strength}} \tag{4}$$

$$\mathrm{EI} = \frac{\text{Total cost of } 1\,m^3 \text{ of mortar}}{28 - \text{day compressive strength}} \tag{5}$$

where m_w represents material's weight (kg), EE_f is Embodied Energy factor, and GWP_f signifies Global Warming Potential factor.

3. Results and discussion

3.1. Microscopic studies of GrP

3.1.1. XRD

The primary components of XRD are identified as quartz (26.6°), calcium sulfide (31.4°), magnesium oxide (42.7°), iron oxide (41.4°), and calcium sulfide (31.4°) as shown in Fig. 1. With help of Inorganic Crystal Structure Database (ICSD), collection code as 90145 indicating the presence of silicon di oxide, collection code as 170905 indicating the presence of magnesium oxide and collection code as 41956 indicating the presence of calcium is noted. GrP can be identified by the presence of excess quartz, as well as by the simultaneous presence of high content of silica and alumina, and by the abundance of aluminosilicate phases as shown in XRD patterns. Meena et al. [57] confirmed the presence of large amount of silica and alumina content in GrP in different forms. Ngayakamo et al. [58] reported the presence of microline, albite, and calcite from GrP, and noted the similar diffraction angles for GrP with respect to Fig. 1. Ramadji et al. [59] reported the presence of calcite and quartz. High quartz concentration and an ideal ratio of silica to alumina content, which are found as aluminosilicate phases, are responsible for the mineralogical properties of GrP [60]. Liu et al. [61] noted the presence of silica, alumina, and ferrous source minerals above 90%.

According to studies by Boadella et al. [62] and Shamsabadi et al. [63], the GrP has a significant concentration of silica and alumina oxides, although its chemical composition varies relatively little. The GrP identifies quartz, biotite, albite, iron oxide, and maghemite as crystalline forms [64]. The observation of quartz, albite, zinnwaldite, microclinium, and caulinite in GrP has been documented in the literature [65]. Quartz and trace amounts of anorthoclase and albite are present in GrP [58]. According to Reddy and Yarakkula [66], the primary components in the GrP are quartz, albite, anorthite, k-feldspars, muscovite, annite, lepidolite, illite, and ferrosilite. With the aid of XRD, Gupta and Vyas [18] discovered that the primary elements identified in the GrP are quartz and feldspar. Ultimately, this study identified quartz, calcium sulfide, magnesium oxide, iron oxide, and calcium sulfide as major mineralogical components of GrP.

Table 2
EE and GW's factors [55].

Material	EE_f (MJ/kg)	GWP_f ($kgCO_2$-eq/kg)
OPC	5.50	0.95
GrP	0.85	0.020
Sand	0.081	0.0051
Water	0.010	0.0010

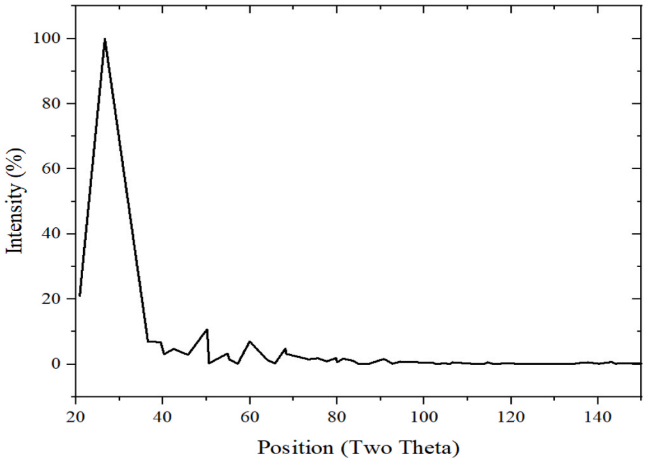

Fig. 1. XRD image of GrP.

3.1.2. FESEM

With reference to the FESEM images shown in Fig. 2, the GrP seemed to have sharp edges (Fig. 2(b)) rather than sponge-like characteristics, and they appeared to be more substantial with a relatively small number of pores on the various surface layers (Fig. 2(a)). Few cracks could be found on the surface of the elements (Fig. 2(c)). From Fig. 2(d), In agreement with the XRD result, it can be noted that GrP sample has sharp edges and that the crystalline structure resembles the presence of silicon oxides. It can be observed from Fig. 2(e) that nanoscale particles were bonded to dispersed from the surface of GrP particles. Fig. 2(f) demonstrates that the elements were three-dimensionally structurally structured units, and the surface depicted crystal solid objects free of pores and with properly arranged atoms, molecules, or ions. The FESEM image indicated the range of GrP particles, which is between 30 μm and 200 nm.

Sapiai et al. [67] reported similar size of particles in the range of 1.5 μm to 60 μm. According to Barra et al. [65], GrP particles exhibit non-spherical form, and their surfaces have rough, superficial textures with acute indentations. The aspect ratio, or the ratio of grain length to grain width, is greater than one for the majority of the particles in Fig. 2, suggesting that the particle has more surface area that is active for reaction [68]. As a pozzolanic material, GrP has more varied particle sizes, which increases its rate of chemical reaction and filling capacity [69]. According to Gupta and Vyas [18], the GrP has a rough surface morphology and irregularly shaped particles. The non-spherical form of GrP particles has distinct points, sharp edges, and a superficially rough surface texture. GrP is suitable as binder material because of these characteristics [65]. Erosion causes the GrP particle surface to develop rounded edges and pebble-like surfaces. The carbonation of the GrP particles is the cause of this alteration in surface roughness [70].

3.1.3. EDS

Fig. 3 shows that GrP possessed higher contents of silicon, aluminium, calcium, and iron. The elements were slightly varied as per location. The elements, which are identified with help of XRD and FESEM, are confirmed with the help of EDS in the terms of concentration of the elements. These results align with relevant study, which reported higher contents of silicon, aluminium, calcium, and sodium in GrP [71]. Smallest particle sizes less than 1 μm are rich in silica, while spherical particles with irregular shape are rich in Fe, Ca, and Al [64]. Reddy and Yarakkula [66] found the presence of silicon and calcium as major elements in the GrP and metals as minor elements in GrP. Kouam et al. [72] noted an increase in silicon and aluminium with increasing

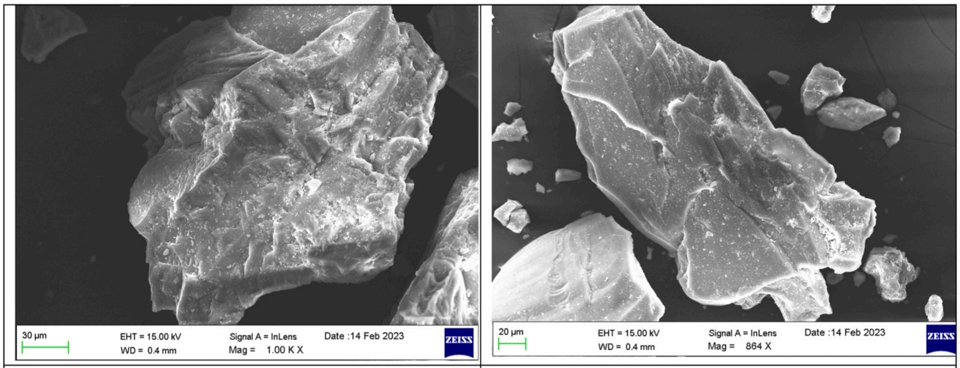

(a) layer surface (b) prismatic shape

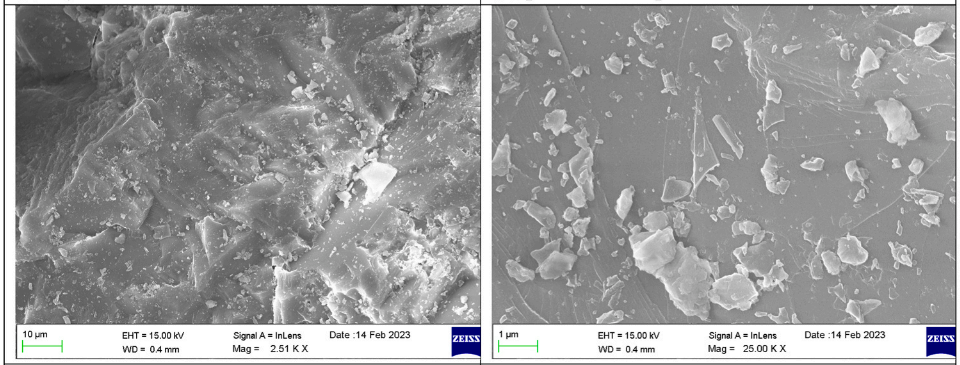

(c) surface with cracks (d) irregular shape

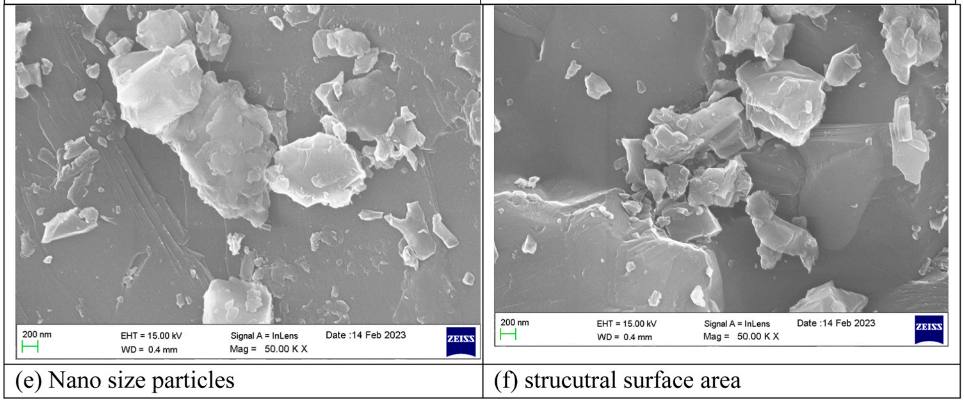

(e) Nano size particles (f) strucutral surface area

Fig. 2. FESEM images of GrP.

grinding time of granite. Thus, the elemental compositions of GrP in this study reveals high contents of silicon, aluminium, calcium, and iron, contributing to the existing literature.

3.1.4. RS

Various pozzolanic minerals in terms of the Raman wavenumber with different intensities are shown in Fig. 4. Notable pozzolanic minerals in GrP, as shown in Fig. 4, are SiO_2, Fe_2O_3, and Al_2O_3 in strong and weak bands. The presence of quartz by the Raman wave number at 134 and 172 cm^{-1} in Fig. 4 is a very strong band [73]. Generally, metallic oxides are present for the Raman wavenumber below 150 cm^{-1}. This might also include different forms of Fe_2O_3 or Al_2O_3. The quartz form demonstrates the presence of SiO_2 in Raman wavenumber at 476 and 524 cm^{-1}, indicating very strong band. Whereas, Al_2O_3 forms strong band at the Raman wavenumber at 642 cm^{-1}. Presence of Fe_2O_3 was noted in strong band of Raman wavenumber at 278 cm^{-1}. Guedas et al. [74] reported similar result, where strong band for pozzolanic materials is obtained with respect to Raman wavenumber.

3.1.5. FTIR

FTIR determines and analyzes the chemical compounds by measuring the absorption or emission of infrared radiation. The method is based on the principle that different chemical bonds absorb or emit light at different frequencies. Fig. 5 displays the chemical bonding of GrP and its wavelength. FTIR vibration bands in Fig. 5 varied from 587 to 1100 cm^{-1}, indicating the presence of metal oxide bonds. Meena et al. [57] noted the vibration bands at 587 and 639 cm^{-1} due to the presence of the Fe-O bond in the iron oxide and Si-O bond stretching vibrations. Peaks at 778 cm^{-1} could be ascribed to Al-O symmetric vibration [57]. Broad strong peak at 1001 cm^{-1}, could be associated with Si-O-Si asymmetric bond for oxygen and non-oxygen bridges [60]. Vibration band at 1096 cm^{-1} corresponds to the oxygen bridging in Si-O-Si in GrP and non-oxygen bridging of SiO_2 in quartz [75]. Vibration band at 1096 cm^{-1} and 1001 cm^{-1} refers to crystalline phase of Si-O bond and presence of asymmetric stretching Si-O-T bonds are assigned at 640 cm^{-1} and 778 cm^{-1} [8]. Garigipati and Malkapuram [76] assigned vibration bands at 640 cm^{-1} and 587 cm^{-1} to quartz and rich content in iron oxides. Broad strong peak nearer to 1010 cm^{-1} can be attributed to Si-O-Si asymmetric vibration and the Si-O symmetric vibration bridge

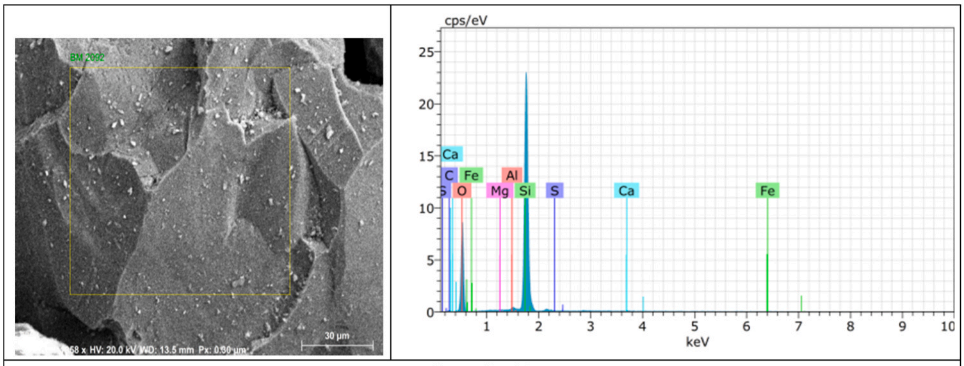

Sample (a)

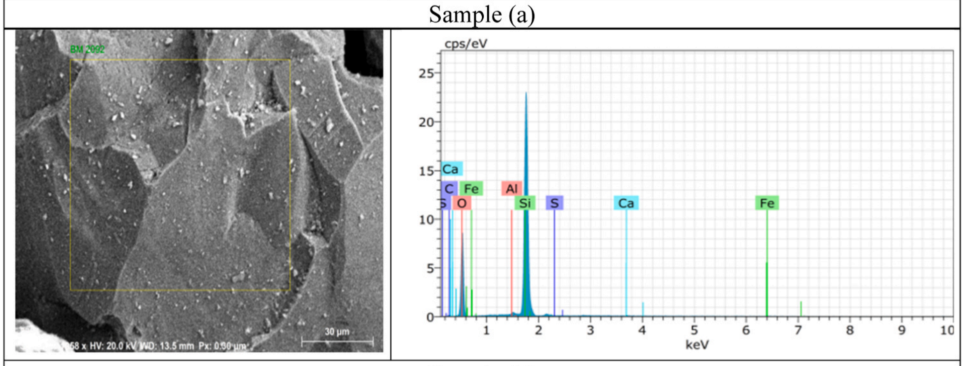

Sample (b)

Fig. 3. EDS of GrP samples.

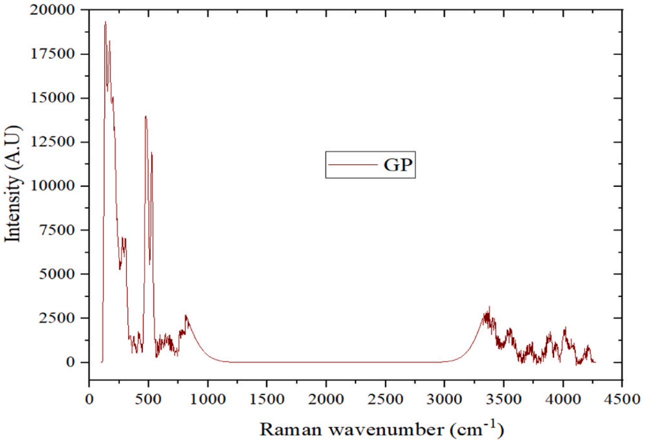

Fig. 4. Raman wavelength for GrP.

[60]. Vibration peaks nearer to 750 cm^{-1} can be assigned to Al-O symmetric vibration, while the peak nearer to 640 cm^{-1} can be attributed to quartz [60]. Vibration peaks nearer to 590 cm^{-1} are assigned to the iron oxides [60]. Hence, the FTIR vibration bands between 587 and 1100 cm^{-1} obtained herein could be related to the presence of the Fe-O bond in the Fe_2O_3 and Si-O-Si asymmetric vibration.

3.1.6. *Thermal analysis*

Fig. 6 shows 1.125% loss in mass in GrP at1000 ºC. The primary ingredients of the granite stone that serves as the source for GrP are crystalline inorganic components [77]. Due to loss of adsorbed water on the surface of GrP particles, there is loss in the mass about 0.6% up-to 300°C, which is also noted in the DSC. And similar loss of mass and its derivate mass was reported by Paul et al. [78]. Heat release around 600°C can be attributed to the change in the phase of plagioclase [79]. Change in the temperature of plagioclases between the 780°C and 820°C was noted by Plevova et al. [80]. GrP starts melt above 1000°C, whereas the melt of GrP at 1110°C was noted by Pan et al. [79] [80]. Oxidation of iron oxide, is noted as loss in the mass at the temperature of 327°C [81]. Change in the crystalline of the quartz from two different forms as α and β which is noted around the temperature 573°C [80]. There is loss in the mass about 1% is noted nearer to 700°C, is due to internal loss of weight to dehydration of the aluminium di oxide and water which is noted in the DSC [81]. The dehydration of inter- and intra-layer crystalline water is responsible for the second set of mass loss, which was detected at 600ºC, amounting to around 0.9%. The oxidation and decomposition of inorganic elements in the GrP was observed around 750ºC, resulting in a mass loss of approximately 1.2%. Loss in the calcite traces is noted as result of decomposition at the temperature 900°C [81]. Eskander et al. [77] noted a similar type of thermal analysis. From Fig. 6, it can be observed that the thermal stability of GrP is very high. Organic silica underwent dihydroxylation and dehydration between 292 ºC and 684 ºC, and Eskander et al. [77] reported a similar type of DTA.

3.1.7. *XRF*

The results of the chemical compositions of GrP and OPC are shown in Tables 3 and 4, which also includes comparisons with other findings from the literature. Ramadji et al. [59] reported presence of high contents of SiO_2, Al_2O_3 and Fe_2O_3. Table 3 shows that SiO_2, Al_2O_3, and Fe_2O_3 add up to more than 70%. According to ASTM C 618 [82] classifications, GrP is categorized as class F pozzolan based on its chemical compositions. Ramadji et al. [59] observed a similar type of chemical makeup in GrP and categorized it as class F. Tawfik et al. [60] found a high amount of alkalis in GrP. GrP appeared reddish due to the high concentration of Fe_2O_3 [60]. The low concentrations of lime and MgO suggest that, in addition to CaO and MgO hydration and carbonation, there is less mass loss from these processes. The contents of SiO_2 and Al_2O_3 in the GrP affects the properties of blended cements [22]. Table 4 represent the chemical composition of OPC 53 grade cement used in this study and compared with the previous studies. The results exhibit similar compositions.

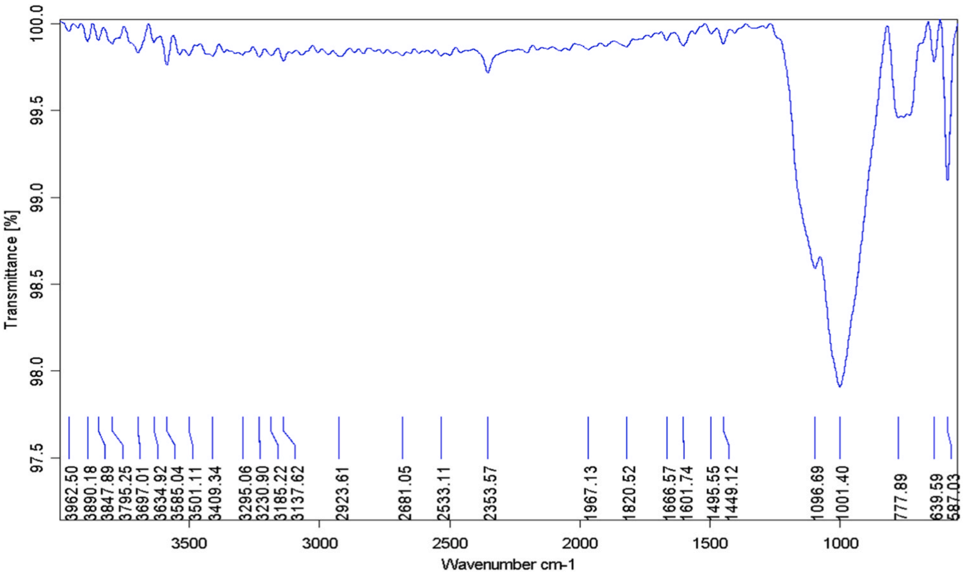

Fig. 5. FTIR for GrP.

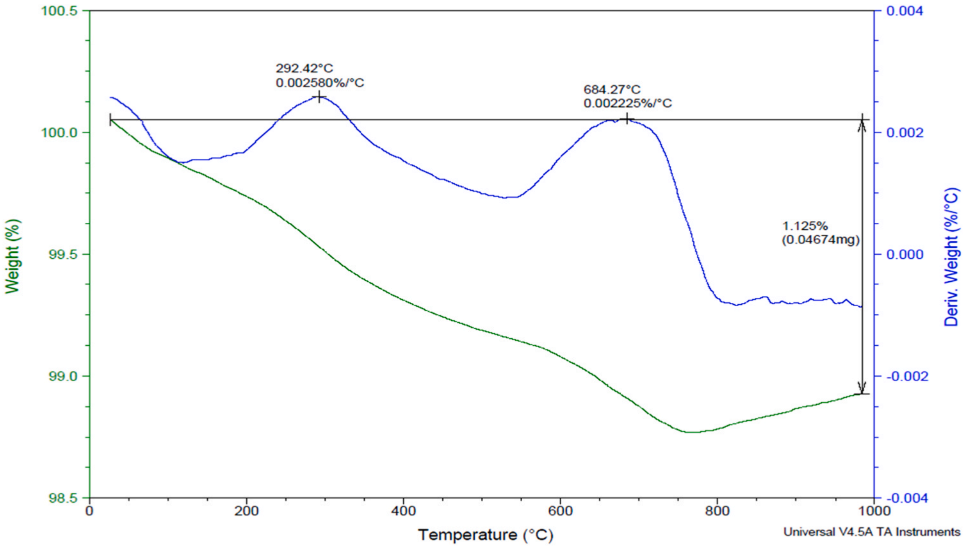

Fig. 6. Thermal analysis of GrP.

Table 3
Chemical compositions of GrP.

Composition (%)	SiO_2	TiO_2	Al_2O_3	MnO	Fe_2O_3	CaO	MgO	Na_2O	K_2O	P_2O_5	SO_3
Present study (GrP)	64.70	0.62	14.10	0.05	6.04	4.86	0.97	4.26	3.38	0.37	0.24
Gao et al. [8]	57.50	0.84	16.68	0.11	5.35	9.13	3.44	2.03	4.52	0.05	0.12
Abreu et al. [64]	65.84	0.33	13.0	0.09	7.12	5.54	0.87	3.14	3.47	0.28	0.09
Ramadji et al. [59]	71.74	0.22	14.91	0.04	1.45	1.14	0.22	3.28	6.58	0.06	0.02
Sapiai et al. [67]	78.91	0.10	10.52	0.18	1.73	2.07	-	-	6.07	-	0.08
Tawfik et al. [60]	69.98	-	14.27	0.50	3.04	15.90	3.30	4.10	5.47	-	-

Table 4
Chemical composition of OPC.

Composition (%)	SiO_2	Al_2O_3	Fe_2O_3	CaO	MgO	Na_2O	K_2O	SO_3
Present study (OPC)	20.22	4.71	4.74	65.67	0.97	0.15	0.48	2.43
Jayachandran & Pillai [83]	18.91	4.52	4.92	66.62	0.86	0.11	0.41	2.52
Nedunuri et al., [84]	17.20	8.40	6.80	64.30	1.20	0.50	0.30	1.40
Chintalapudi & Pannem [85]	18.91	4.51	4.94	66.67	0.87	0.12	0.43	2.50

3.2. Physical properties of GrP

The result of GrP's specific gravity was 2.55. According to Vijayalakshmi et al. [13], a higher specific gravity is associated with a larger GrP grain size. The specific gravity of GrP decreases with increasing grain size, causing more air spaces to form between the grains [22]. GrP grain characteristics are estimated using the grain size and morphological structure. The specific gravity and pozzolan specific area are directly correlated [86]. Specific surface area of GrP is observed as 390 m^2/kg and Blaine's surface area whereas for the cement it is noted as 360 m^2/kg. In literature, it is noted that the Blaine's surface area of GrP was noted in the range between 380 m^2/kg to 680 m^2/kg [87]. Barra et al. [65] observed that the fraction of particles smaller than 37 μm and 20 μm were 43.8% and 22.9%. Based on the provenance of the stone, the specific gravity of GrP has been reported in the literature to range from 2.36 to 2.72 [88]. The micro and nanoparticle size of pozzolan on the pace of hydration reaction also affects the specific gravity [86,89]. For their study, Gupta and Vyas [18] employed GrP with a fineness modulus of 0.95 and a specific gravity of 2.60.

The water absorption of GrP is discovered to be 4.1%. Increased water absorption is associated with the presence of defects and micro cracks on the surface of the GrP particle, which is noted from the Fig. 2. The amount of water in the blended cement mixture increases because of these fissures because they absorb more water [22]. Using the LA-960 Laser particle size analyzer, the GrP's particle size distribution (PSD) is displayed in Fig. 7, and it was discovered that the GrP's average diameter was 18.88 μm. The selection of different sizes of GrP particles helps enhance the density of the blended cementitious mixture, contributing to the hardened properties. Formation of nucleation cite at the surface of GrP particles depends on the particle sizes and the formation of pozzolanic reaction. In terms of the GrP's size and fineness, longer grinding times might not yield the best results. This is caused by the cohesion forces that cause the GrP particles to agglomerate on the walls of the drums and grinders, forming a paste, as well as the electrostatic interaction forces that cause the very fine GrP particles to contact with one another [71]. Nonetheless, the surface area of GrP increases with increasing grinding time [71,90]. Hence, the GrP particle size has a significant influence on the GrPBC mixes [91].

3.3. GrPBC properties

3.3.1. Specific gravity

Fig. 8 depicts an increase in the consistency of GrPBC with increasing GrP content in the mix. This could be related to the decrease in specific gravity due to lower specific surface area of GrP compared to the OPC as reported in FESEM (Fig. 2). Morphological characteristics of GrP demonstrated the sharp edge with particle size larger than OPC, resulting in decrease in the specific gravity. Specific gravity of GrPBC is lower than OPC; this is due to larger volume of GrP (Larger particle size of GrP compared to that of OPC) [92]. The specific gravity of OPC is 3.148, and for GrPBC, it varies from 3.132 to 1.945 as partial replacement of OPC by GrP varied from 4% to 40%. Compared to specific gravity of OPC, the drop in the specific gravity of GrPBC are 0.51%, 1.33%, 2.73%, 4.83%, 7.56%, 11.21%, 15.92%, 21.82%, 29.19%, and 38.22% for 4%, 8%, 12%, 16%, 20%, 24%, 28%, 32%, 36% and 40% wt % GrP partial replacement for OPC. Due to a decrease in specific gravity, there is increase in the volume of GrPBC, increasing the water content in the mix [90].

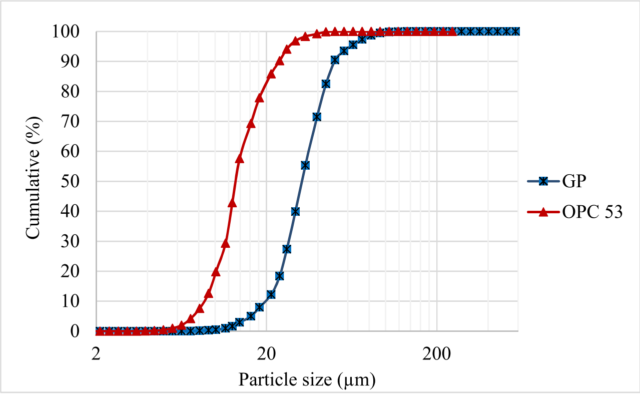

Fig. 7. PSD of GrP and OPC.

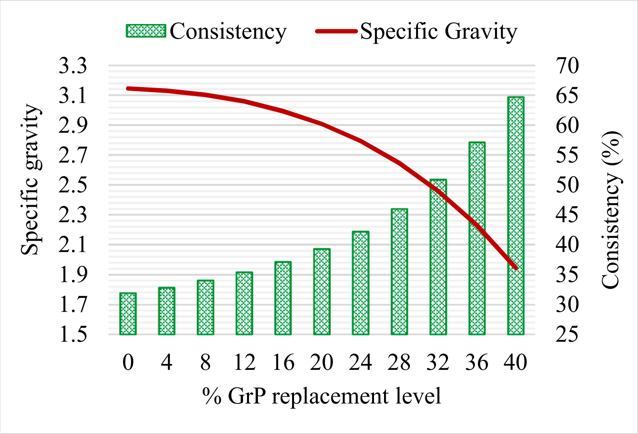

Fig. 8. Specific gravity and consistency of GrP.

Knop and Peled [93] reported the influence of particle size of pozzolanic materials on the hydration of the pozzolanic material. Heat of hydration at early stages of blended cement depends on the particle size of the pozzolan. Hence, there is direct relationship between the specific gravity and particle size, particle size and hydration rate heat of pozzolan, and particle size and surface area of particle itself [93]. Smaller particle size exhibits higher surface areas, resulting in the reduction of hydration degree compared to that of the larger particle size with lower surface area of particles. Some of the fine particles in pozzolan act as inert in age's hydration of blended cement, which does not participate in early hydration, but on later stage, it starts reacting [94].

3.3.2. Consistency

It is evident from Fig. 9 that a rise in GrP content led to an increase in GrPBC's consistency. About 3–103% of the water content increased relative to the control mix for 4–40 wt% of GrP as a partial replacement for OPC. To ensure consistent workability, the amount of water required generally increases as GrP increases because of the morphological

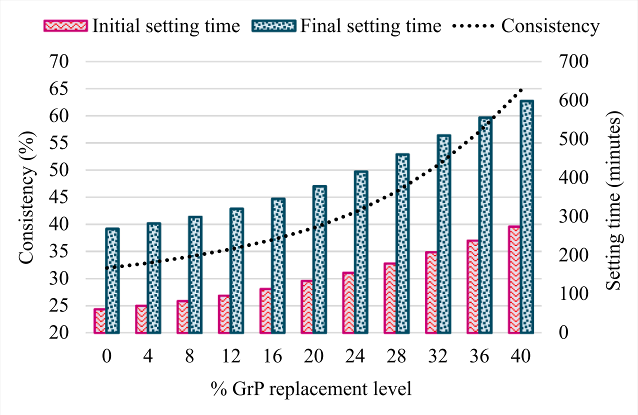

Fig. 9. Consistency and setting time of GrP.

properties of the GrP particles. The amount of water surrounding GrP particles increases with a higher specific surface area of the grain particle. More water is needed for GrP particles with a greater surface area to retain the same workability in GrPBC mixes. Additionally, the pores and spongy features that develop in a few spots on the GrP surface determine the extra water needed.

With high specific surface area, GrP particles have stronger binding strengths with aggregates and cementitious materials [22,68]. Specific surface area of GrP grains is a significant characteristic that stimulates the interaction between the cementitious materials and the aggregates [22,68]. Higher specific area of GrP results in a higher requirement for water [22,68]. Due to its high absorption capacity, GrP acts as a natural moisture reservoir to facilitate the continual hydration of cement during mixing. This reservoir generates calcium silicate hydrate, which gives the concrete a denser matrix, reduced porosity, and enhanced strength [95]. Specific surface area has a positive effect on the mechanical properties of the cementitious composites. Larger specific surface area of GrP grains leads to increase the ITZ between the GrP and other particles, thereby increasing the density of composites and increases the mechanical properties of composites [22]. Therefore, specific surface area has a direct effect while specific gravity has an indirect effect on the blended cement mixtures. The diluting effect of GrP on the cementitious system is responsible for the observed decrease in heat of hydration with increasing GrP content [96]. Because GrP's specific gravity is lower than OPC's, it produces a larger volume and necessitates more water. Consequently, blended cement mixes have a higher consistency, as documented in literature [97]. More water is added as a result, and setting times are extended. Lower pozzolan hydration rate is another factor contributing to longer setting times with increased GrP content [98].

3.3.3. *Setting times*

It can be seen from Fig. 10 that OPC showed a shorter setting time than the blended cements. The OPC contains a larger concentration of tricalcium silicate and tricalcium aluminate phases than GrPBC, which accounts for the quicker setting time [99]. Tricalcium silicate rapidly hardens in the presence of water, resulting in the early setting time [100]. A larger GrP particle size causes a longer time to hydrate, which lengthens the GrPBC's setting time [93]. The setting time for GrPBC is longer because the average particle size of GrP is slightly higher than that of OPC. Compared to reference mix, increase in initial setting time was 14.75%, 34.43%, 57.38%, 85.25%, 119.67%, 154.10%, 193.44%, 240.98%, 290.16%, and 349.18% at partial replacement of OPC by 4%, 8%, 12%, 16%, 20%, 24%, 28%, 32%, 36% and 40% of GrP. Whereas, for the final setting time, the increase in time compared to control mix was 5.22%, 11.57%, 19.40%, 29.10%, 41.04%, 55.22%, 71.64%, 89.93%, 89.93%, 107.09%, and 123.13% for the partial replacement of OPC by 4%, 8%, 12%, 16%, 20%, 24%, 28%, 32%, 36%, and 40% of GrP.

The reasons for these increases in setting times are the GrP particle size, the mix temperature, and the mix's water content. Hydration of tricalcium aluminate generates substantial amount of heat that increase the setting temperature, resulting in quicker setting behavior of OPC compared to blended cement. Setting time of OPC decreases with increase in the temperature [101]. The GrPBC's longer setting time is attributed to the fact that GrPBC contains GrP that raises water demand of GrPBC mix. Higher water demand of GrPBC retards the setting behavior of cement pastes and reduces the rheology/cohesiveness of the GrPBC pastes [102]. Longer initial and final setting times were the outcome of increasing the GrP content in blended cements. The slow setting time is caused by the steady decrease in the quantities of tricalcium silicate and tricalcium aluminate components. The delayed nature of GrP responses is the reason for the lengthy setting time of GrPBC. Pozzolanic reactions in GrPBC can only occur when calcium hydroxide is liberated, either from the hydration of OPC or from its availability in the matrix system [103]. The pozzolanic reaction of GrP is slow, so the setting behavior associated with this reaction is low. The slow pozzolanic reaction retards the setting times in GrPBC [99]. There is also increase in the initial and final setting times due to the presence of more amount of insoluble residue in the GrPBC. Increased GrP content causes a decrease in cement content, which prolongs setting times and causes GrPBC to hydrate slowly [91].

3.3.4. *SAI*

Fig. 11 shows that an increase in GrP content increased the SAI of GrPBC up to 20% at 7- and 28-days curing. The increase in compressive strength for GrPBC was 1.02, 1.05, 1.08, 1.11, 1.05, 0.96, 0.92, 0.86, 0.77, and 0.67 times higher than reference mix for 4%, 8%, 12%, 16%, 20%, 24%, 28%, 32%, 36%, and 40% of GrP substitutions at 7 days curing. At 28 days, the compressive strength of GrPBC was 1.04, 1.05, 1.09, 1.11, 1.06, 0.99, 0.94, 0.89, 0.83, and 0.71 higher than the control mix for 4%, 8%, 12%, 16%, 20%, 24%, 28%, 32%, 36%, and 40% of GrP substitutions. The GrP's filler effect in the cementitious system is initially responsible for the increase in compressive strength. Afterwards, the GrP particle takes part in the pozzolanic reaction. These are dependent upon the hydration reaction that generates calcium hydroxide and the presence of crystalline mineralogical compositions from the GrP. Juenger and Siddique [104] suggested that the creation of a nucleation site on the surface of GrP occurs at later ages, and that the filler effect in the cementitious matrix is the cause of the low reactivity of GrP at earlier ages. This nucleation site makes space for the hydration products to precipitate after it takes part in the pozzolanic reaction. This is the reason, when GrP is used as a partial replacement for OPC; higher strengths are recorded at later ages [105].

Fig. 12 illustrates the rise in SAI for the 7- and 28-day compressive

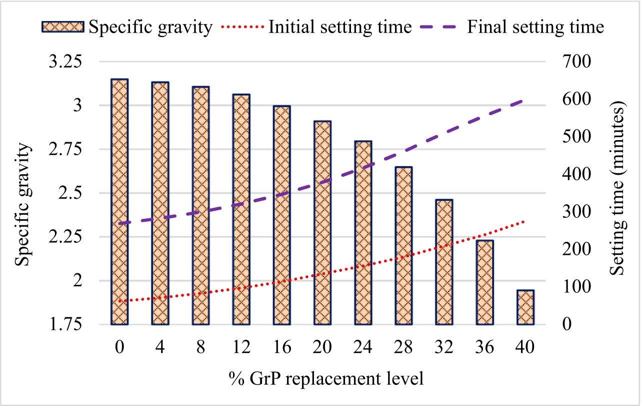

Fig. 10. Specific gravity and setting times of GrP.

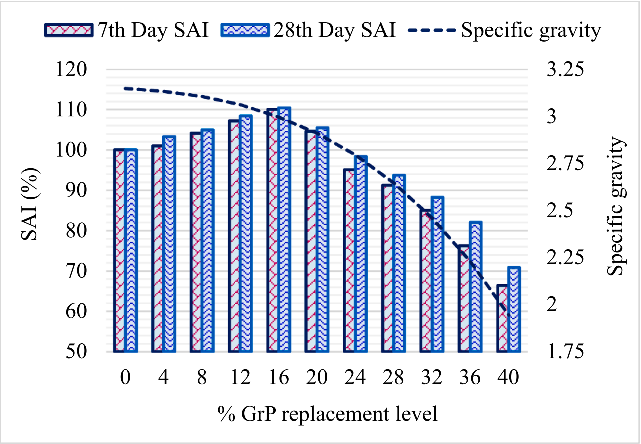

Fig. 11. SAI and specific gravity of GrP.

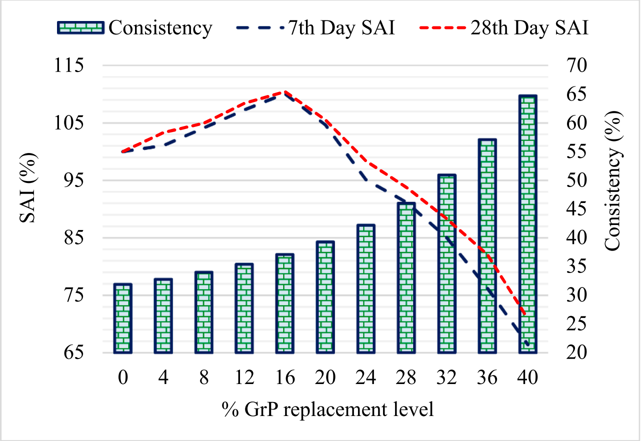

Fig. 12. SAI and consistency of GrP.

strengths with respect to consistency that occurred with a GrP content increase from 4% to 20%. An increase in SAI is caused by the filler effect of GrP; on the one hand, GrP functions as micro aggregates, reducing porosity and enhancing mechanical characteristics [8]. Calcium hydroxide released from hydraulic reactions in the blended mixes increased with increasing GrP content up-to 20%; this participated in the pozzolanic reaction and increased the strength properties. However, as GrP increased above 20%, the diluting action caused a drop in calcium hydroxide and reduced the strength index [95]. Contribution of strength properties is due to the amorphous silica and alumina from pozzolan dissolve in the pore solution. Hence, the beginning of hydration or pozzolanic reaction depends on the reactivity of GrP and the availability of calcium hydroxide [95].

Calcium hydroxide from hydration reaction or calcium hydroxide in cement matrix system reacts with pozzolanic minerals from GrP, in the presence of water to form calcium silicate hydrate and calcium aluminate hydrate, contributing to the hardened properties of GrPBC [99]. Ultimately, this study establishes that 20 wt% GrP replacement with OPC is the optimum replacement level for achieving suitable mechanical strength.

3.4. *Development of relationship between compressive strength and water to binder ratio*

3.4.1. *Regression modelling*

Development of statistical models are established between the independent and dependent variables. There are several statistical models available in the literature to analyze the relationship between the variables. Most of the statistical models have one dependent variable as a constant and other as independent variables [106]. These dependent and independent variables depend on the numerous factors like type of binding material, curing period, water to binder (W/B) ratio, etc. Thus, in this model, the relationship between the variables based on the physical, chemical, and morphological characteristics of constituents are put into consideration [107]. In addition, the relationship is applicable for a large range of experimental data with different binders, water content, etc., available in the literature. Efficiency of proposed and derived relationships through regression analysis can be assessed by the Integral Absolute Error (IAE, %) [108]. This is proposed in Eq. (6):

$$\mathrm{IAE} = \sum \frac{\left\{ [O_i - P_i]^2 \right\}^{1/2}}{O_i} \tag{6}$$

where O_i is the observed value and P_i is the predicted value from the regression analysis. Relative deviations of data from the regression equation are measured by IAE. The range from 0% to 10% may be regarded as IAE acceptance limits for fit of regression equations.

3.4.2. *Development of relationship between the compressive strength and water to binder ratio*

Regression models were carried out to establish a relationship between the compressive strength and W/B ratio. The findings of these analyses are presented in Table 5. The values of coefficient of determination (R^2) and IAE for various regression equations are shown in Table 2. The values of N and M, as shown in Table 5, are constants obtained from Fig. 13 using general regression analysis. The best relationship shows an R^2 value that is closer to one and an IAE value that is closer to zero [109]. General fit regression analysis for the Equations (7)-(11) are developed with help of Fig. 13. Average value of IAE is considered as overall IAE. Based on the R^2, Equations (7)-(11) yielded a strong relationship between f_{cmk} and W/B ratio for both 7 and 28 days. In terms of IAE, the lowest value was noted for Equation (8). Hence, Equation (8) provides reliable and accurate correlation in terms of R^2 and IAE. Therefore, there is a transition point in the relationship between compressive strength and water to binder ratio.

3.4.3. *Validation of the model*

Water to binder ratio, compressive strength from literature, and proposed equation are necessary to assess the validity of the proposed model [109]. Validation aids in determining whether the proposed model is appropriate for use in real-life applications [104]. Model validation is a necessary step in the complex task of simulation. The W/B ratio and 28 days compressive strength are summarized in the Table 6, consisting of actual and predicted compressive strength from the literature [87,110–112]. It can be inferred that the proposed model is utilized to forecast compressive strengths greater than 50 MPa. The range of compressive strength and the curing period influence the proposed model.

3.5. *Derivation of constants for relationships using regression analysis*

According to previous studies, there is a correlation between compressive strength and water binder ratio [87,113–115]. Amongst other advantages, regression analysis results in cost reduction and natural resource preservation. Several studies relate the compressive strength of concrete or mortar to the water binder ratio [87,114–116]. Few of the relationships available in literature are illustrated in Eqs. (12)-(15):

$$f_{\mathrm{cmk}} = \left[\frac{\mathrm{A}}{\mathrm{B}^{\mathrm{W/B}}} \right] \tag{12}$$

$$\mathrm{f}_{\mathrm{cmk}} = \mathrm{K}_1 \left(\frac{\mathrm{V_B}}{\mathrm{V_B} + \mathrm{V_w} + \mathrm{V_a}} \right)^2 + \mathrm{K}_2 \tag{13}$$

$$\mathrm{f}_{\mathrm{cmk}} = \mathrm{n}_1 [\mathrm{W/B}]^{\mathrm{n}_2} \tag{14}$$

$$\mathrm{f}_{\mathrm{cmk}} = \left(\frac{C}{W/B} \right) + D \tag{15}$$

where f_{cmk} is cube compressive strength (MPa) of blended cement at various days of curing, A and B are constant which is used as parameters to calculate the strength, V_B is weight of binder (grams), V_w is weight of water (grams), V_a is weight of aggregates (grams), K_1 and K_2 are constants estimated as the strength parameters, n_1 and n_2 are constant, and it is calculated as strength parameters, C and D are constant, and it is calculated as strength parameters. Jagadesh et al. [106] reported the discussion of the derivation of constants for the relationship between the properties.

General regression modeling demonstrates the relationship between the compressive strength and the W/B ratio for various curing days and computes the coefficient of relation value without varying any parameters. Fig. 14 (a) shows a stronger correlation between compressive strength and W/B ratio for 7 days compared to 28 days. Fig. 14 compares

Table 5
Results of general static models and calculated R^2 and IAE.

Equation	Relationship	7 Days				28 Days			
		N	M	R^2	IAE	N	M	R^2	IAE
(7)	$f_{cmk} = \left[\frac{N}{W/B^M}\right]$	21.167	0.62	0.81	5.24	33.29	0.52	0.80	4.68
(8)	$f_{cmk} = \mathrm{N}[1 - W/B]^M$	54.967	0.72	0.89	3.36	74.87	0.61	0.88	3.06
(9)	$f_{cmk} = \mathrm{N}(W/B) + M$	57.811	19.87	0.87	181.16	46.63	9.98	0.89	96.29
(10)	$f_{cmk} = \mathrm{N}\left[e^{\left(\frac{W}{B}\right)M}\right]$	65.744	-1.39	0.86	99.97	87.06	-1.18	0.85	99.97
(11)	$f_{cmk} = \left(\mathrm{M}\sqrt{W/B}\right) + N$	-62.72	77.41	0.87	100.05	-77.59	103.37	0.85	100.07

Feret [114] to Abram [113] and reveals a greater R^2 value. Whereas, the R^2 value for Feret [114] was noted in Fig. 14 (b) for the correlation between the mix ingredients and the compressive strength. From general regression modelling for various laws related to compressive strength and W/B ratio, the highest coefficient of relation was noted for 28 days compressive strength compared to that of 7 days. Feret's law in Fig. 15 (a) and Bolomey's law [115] in Fig. 15 (b) among other laws displayed satisfactory outcomes with the highest R^2 value. The constants for the various relationship between the compressive strength and water to binder ratio for the general static modelling can be arrived from the Fig. 14 and Fig. 15.

3.6. *Lifecycle assessments*

3.6.1. *Embodied energy*

Fig. 16 displays the EE of GrPBC as well OPC mortar mixes, referencing Tables 1 and 2, and Eq. (2). According to the findings, the EE decreased as the mortar mix's GrP content increased. The GrPBC mortar samples had a lower EE than the OPC mortar samples. In comparison to the control (OPC) mortar, which produced 2.804 MJ-eq/m^3, the GrPBC mortar samples produced embodied energies of 2.713 and 1.895 MJ-eq/m^3 at 4 and 40 wt% substitutions of GrP. This could be explained by the fact that GrP has an EE coefficient that is 84.55% lower than OPC's, meaning that GrP is a low EE building material. This result supports earlier research that found blended concrete's EE decreased when recycled waste components were incorporated [45,117]. Abubakar et al. [117] observed a 3–12% decrease in EE when 5–20% of the corncob ash was replaced with OPC in the production of blended cement concrete. In a similar vein, Oyebisi et al. [45] found that replacing OPC with 5–20 wt % of Sheanut Shell Ash (SSA) decreases EE by 3–13%. Their research revealed that the EE coefficients of shea nutshell ash and corncob ash were 76% and 73% lower than OPC coefficient. Lovecchio et al. [118] found that when OPC was substituted with Ultrafine Fly Ash (UFA) at a rate of 8–12% and 40–60%, the EE dropped by 3–5% and 16–28%. The results herein clearly showed that, at an ideal replacement of OPC with 20 wt% of GrP, the energy-reducing potential of cement-based mortar incorporated with GrP is achievable at an optimal level to compete favorably with OPC mortar counterpart. Thus, appropriate design of GrPBC mixes is necessary to reduce their energy implications and improve the sustainability of building materials.

3.6.2. *Global warming potential*

The global warming results of the OPC and GrPBC mortar samples are given in Fig. 17, applying the information in Tables 1 and 2, and Eq. (3). As the GrP concentration rose, the mix's GWP decreased, as seen in Fig. 17. In comparison to the control (OPC) mortar, which produced GWP of 0.460 kgCO_2-eq/m^3, the GrPBC mortar samples generated GWPs of 0.442 and 0.283 kgCO_2-eq/m^3 at 4 and 40 wt% substitutions of GrP. This result could be attributed to the probability that OPC mortar mixes outperform GrPBC mortar mixes in terms of the total effects of different greenhouse gas emissions that contribute to global warming [109]. Table 2 displays that OPC's global warming coefficient is 97.90% higher than GrP's. These results validate the earlier studies, where the partial replacement of OPC with 5 wt% slag and corncob ash and 7–48 wt% UFA reduced the EE by 5% [45] and 8–60% [118]. A further 34% reduction in global warming potential was achieved by substituting 50% of ground-granulated blast furnace slag for OPC [118]. According to Robayo-Salazar et al. [119], producing green concrete with slag in place of OPC reduces greenhouse gas emissions by about 45%. In contrast, Lovecchio et al. [118] found that partial substitutions of OPC with 2% each of Nano silica and Nano calcium carbonate increased GWP by 1.49 and 12.58%. Global warming and other climate-related concerns can be lessened by using recycled and environmentally friendly waste products, as highlighted by Sagheb et al. [120]. The results obtained here make it clear that, as compared to using OPC to produce GrPBC mortar, recycling GrP offers potential for reducing global warming. Therefore, GrP can be applied in the building sector to create communities and cities that are safe and sustainable while reducing the consequences of climate change.

3.7. *Sustainability index*

The SI of mortar mixtures is displayed in Fig. 18, using Eq. (4). According to Fig. 18, when the mix's GrP content rose from 4% to 20%, the SI declined. The SI increased when the GrP content rose from 24% to 40%. In comparison to OPC mortar mix, which has 0.0110 kgCO_2-eq/m^3/MPa, substituting OPC with 4–20 wt% GrP yields SI of 0.0102–0.0085 kgCO_2-eq/m^3/MPa. However, the SIs of 0.0087–0.0098 kgCO_2-eq/m^3/MPa were found by substituting OPC with 24–40 wt% GrP. The reasons may stem from the mortar mix's comparatively decreased GWP, EE, and SAI at a 24–40% GrP substitution. These results showed that 4–20 wt% GrP replacement with OPC in GrPBC mortar mixes is more environmentally friendly than 24–40 wt% GrP inclusion, because a product's sustainability increases with a lower SI [45,46]. A related study found that the SI decreased with increasing SSA content by 5–20%, making SSA a sustainable construction material with adequate structural strength [46]. The results of this investigation are in line with those of Rahla et al. [121], who asserted that the sustainability of concrete is enhanced by SCMs (slag, fly ash, and silica fume). In contrast to the control sample (100% OPC), which had a 0.51 sustainability score, there were approximately 0.73–0.82, 0.61–0.67, and 0.51–0.52 sustainability scores for 30–40% slag, 5–10% silica fume, and 10–20% fly ash. Braganca et al. [122] stated that employing SCMs in part instead of OPC reduces the quantity of cement needed to produce concrete, boosting sustainability and preserving or even enhancing the material's durability and mechanical properties. Adoption of GrP resulted in a drop in the SI of mortar produced, offering a lasting advantage because of its potential to reduce the EE and GWP of mortar manufacture. Ultimately, this study recommends that 20 wt% of GrP be substituted for OPC in order to maintain sustainability without lowering the GrPBC mortar's strength activity index.

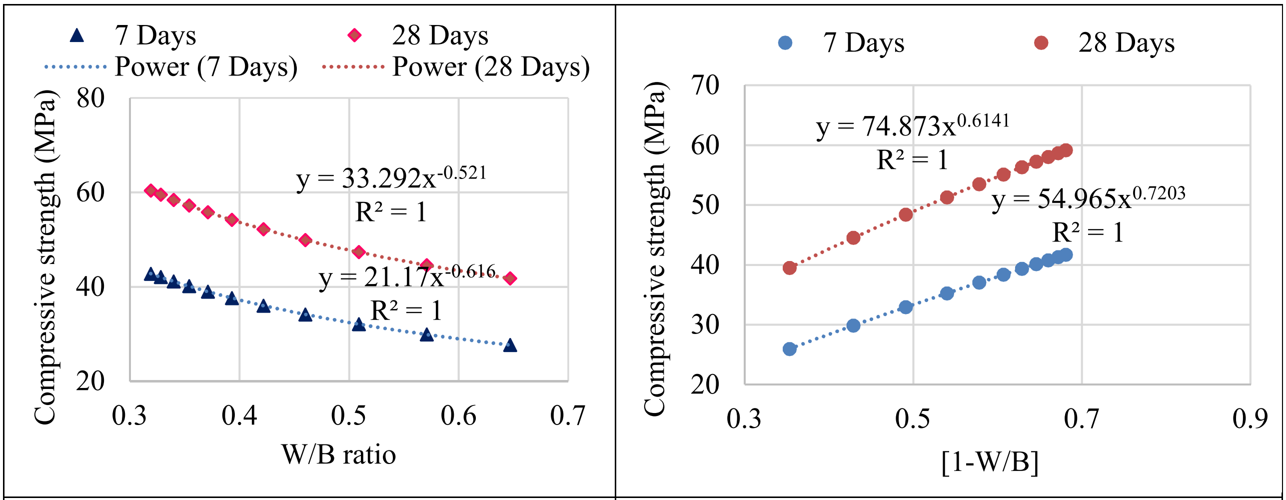

(a) Regression analysis for Equation (7)

(b) Regression analysis for Equation (8)

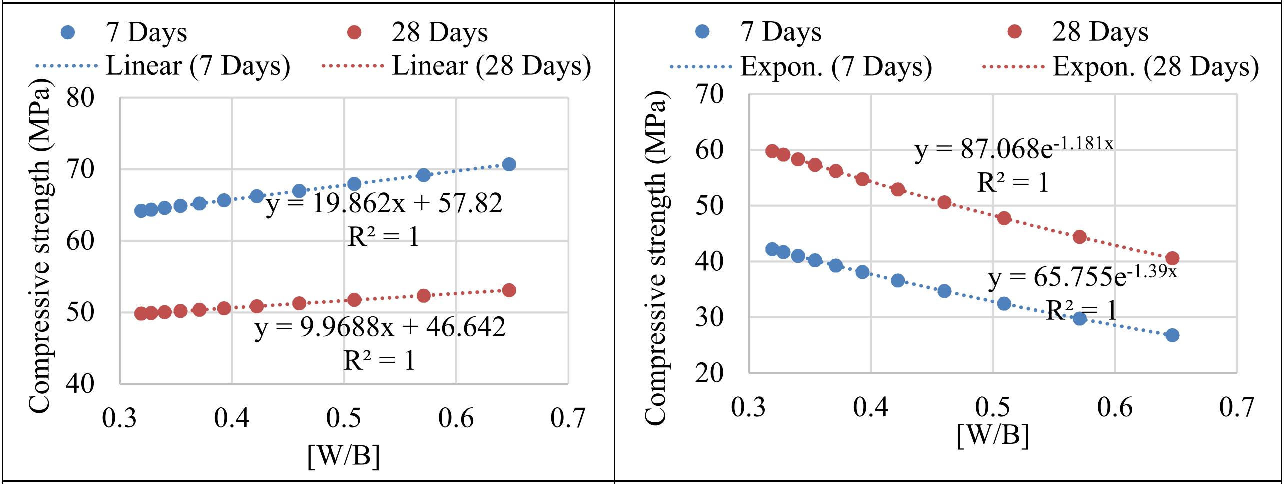

(c) Regression analysis for Equation (9)

(d) Regression analysis for Equation (10)

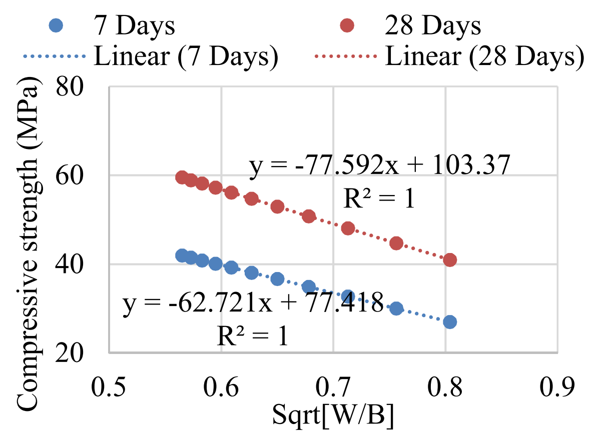

(e) Regression analysis for Equation (11)

Fig. 13. Development of new equation with help of regression analysis.

3.8. *Economic index*

The EI of the GrPBC mixes is shown in Fig. 19. The results, as illustrated in Fig. 19, demonstrated that the EI of GrPBC mixes dropped as the GrP percentage in the mix increased from 4% to 36%. Compared to OPC mortar, this led to a cost decrease of between 5.95% and 19.19%. However, as the GrP content in the mixture rose to 40% the EI increased by 4.13%. According to Fig. 19, the lowest EI value fell between 16 and 20 wt% GrP substitution. This shows that GrP is profitable at 20% optimal replacement. The reasons for these outcomes in terms of the compressive strength of the mortar could be related to the total cost of manufacture. At a substitution rate greater than 20 wt% GrP, the compressive strength of GrPBC mortar started declining. Bajpai et al. [123] reported similar findings, who discovered that the manufacturing of blended cement concrete was 11–18% cheaper due to the use of SCMs (fly ash and silica fume). Thus, the best replacement level, according to

Table 6
Validation of 28-day compressive strength using Equation (8).

Present Study		**Jagadesh et al.** [106]			**ElNemr** [111]			**Singh et al.** [87]			**Rao.** [112]		
W/B	f_{cmk}	W/B	f_{cmk}		W/B	f_{cmk}		W/B	f_{cmk}		W/B	f_{cmk}	
			Actual	Predicted		Actual	Predicted		Actual	Predicted		Actual	Predicted
0.319	54.6	0.67	28.26	53.32	0.4	25.6	50.6	0.5	22.46	51.62	0.35	61.5	50.13
0.328	56.4	0.678	29.03	53.4	0.5	24.6	51.6	0.6	22.99	52.62	0.4	54.87	50.63
0.340	57.3	0.685	30.07	53.47	0.6	20.5	52.6	0.7	20.85	53.62	0.45	59.47	51.13
0.354	59.2	0.695	28.81	53.57	0.7	16.9	53.6	0.8	19.94	54.62	0.50	50.92	51.62
0.371	60.3	0.71	28.09	53.72	0.8	14.1	54.6	0.9	18.75	55.62			
0.393	57.6	0.723	26.59	53.85				1	17.2	56.61			
0.422	53.7	0.738	23.94	54.0				1.1	16.89	57.61			
0.460	51.2							1.2	15.36	58.61			
0.509	48.2												
0.571	44.8												
0.647	38.7												

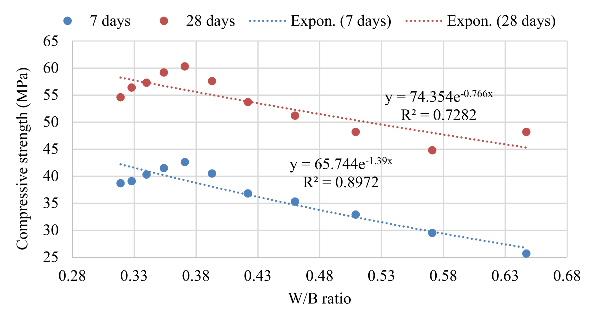

(a) Abram's law

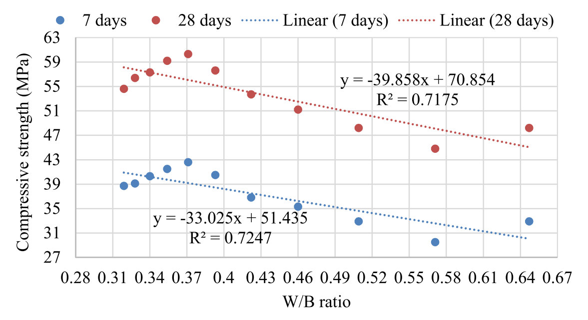

(b) Feret's law

Fig. 14. Relationship between compressive strength and W/B ratio from literatures by general static modelling (Abram's law & Feret's law).

this study, should be 20 wt% GrP to maintain the compressive strength of blended cement mortar.

4. Conclusions

This study characterizes the microscopic properties of GrP using XRD, FESEM, EDS, RS, FTIR, Thermal analysis, and XRF. In addition, the study investigates the effects of GrP on the physical and mechanical properties of GrPBC via rheological properties and SAI. The impacts of GrP on EE and GWP of GrPBC mortar mixes were assessed using the inventory of carbon and energy. The sustainability and economic indexes of GrPBC mixes were evaluated and the relationship between the compressive strength and W/B ratio was modelled. Based on the study's findings, the following conclusions can be drawn:

i. The addition of GrP improves the microscopic characteristics of the GrPBC by enhancing their fresh and hardened properties.

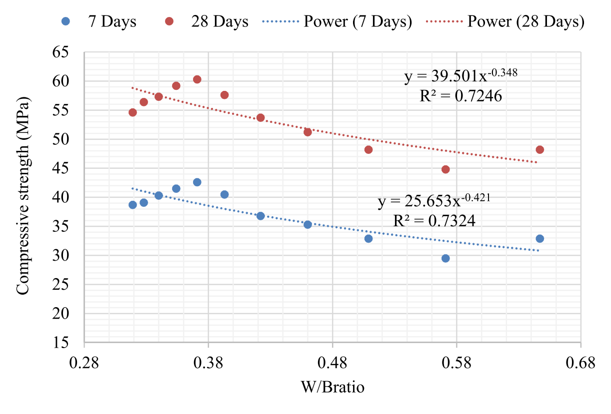

(a) Singh's law

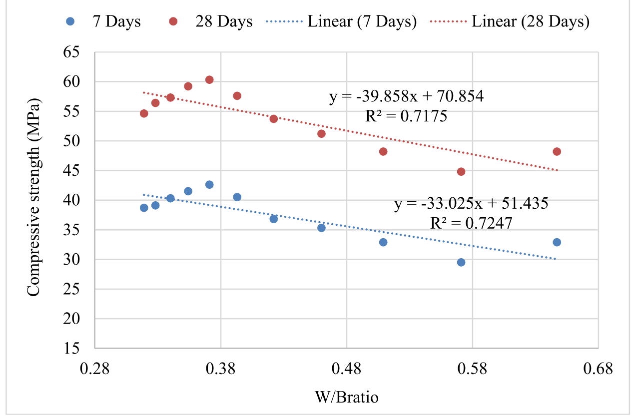

(b) Bolomey's law

Fig. 15. Relationship between compressive strength and W/B ratio from literatures by general static modelling (Singh's law & Bolomey's law).

ii. GrP possesses high contents of silica and alumina, making it a good pozzolanic material with active reactivity in the cementitious matrix.

iii. An increase in GrP content decreases the specific gravity, increases the consistency, and prolongs the setting times of the GrPBC.

iv. The SAI of GrPBC increases with increasing GrP content. However, the optimum replacement level of GrP content in the mix is found to be 20 wt%.

v. The correlation between the compressive strength and W/B ratio of GrPBC exhibited good performance metrics with IAE and R^2 yielding 3.06 and 89% at 28 days curing.

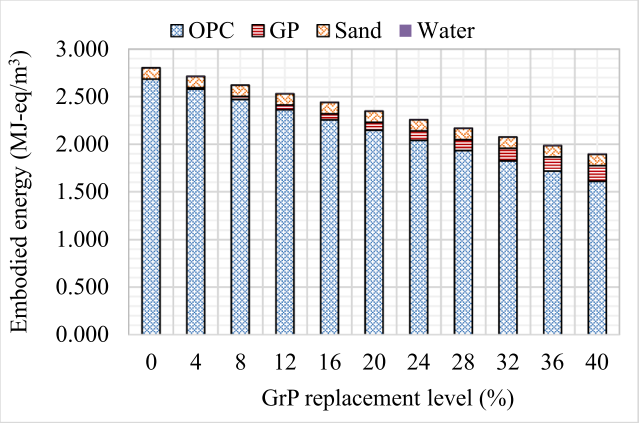

Fig. 16. EE of GrPBC mortar mixes.

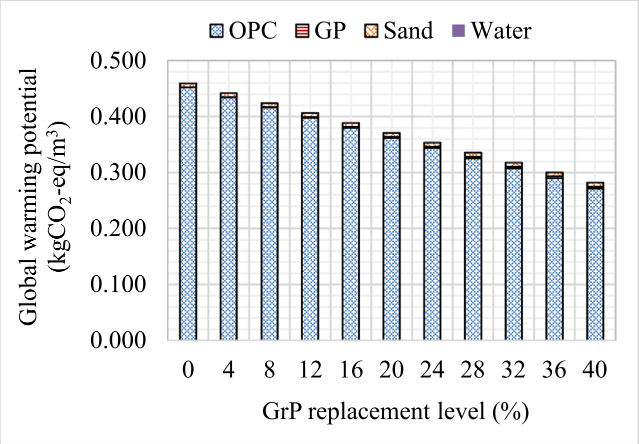

Fig. 17. GWP of GrPBC mortar mixes.

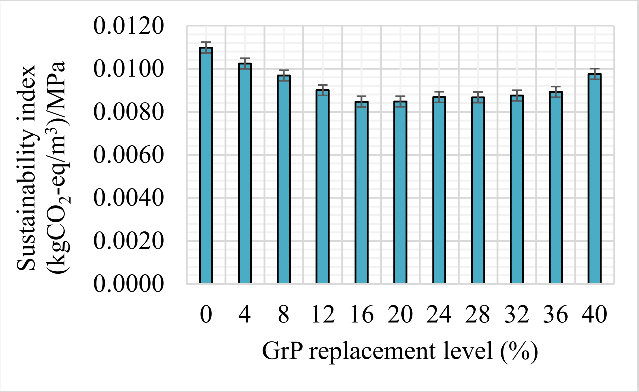

Fig. 18. SI of GrPBC mortar mixes.

vi. There exists a better correlation between the compressive strength and W/B ratio of GrPBC using Abram's law compared to Feret, Singh, and Bolomey's laws at 7- and 28-days SAI.
vii. EE and GWP decreased by approximately 4–33% and 3–39% as GrP content in the GrPBC increased from 4 to 40 wt%.
viii. The best sustainability and economic viability of GrPBC are produced by a 20 wt% GrP substitution, which is almost 23% higher in sustainability score and 19% higher in economic value than OPC mix.

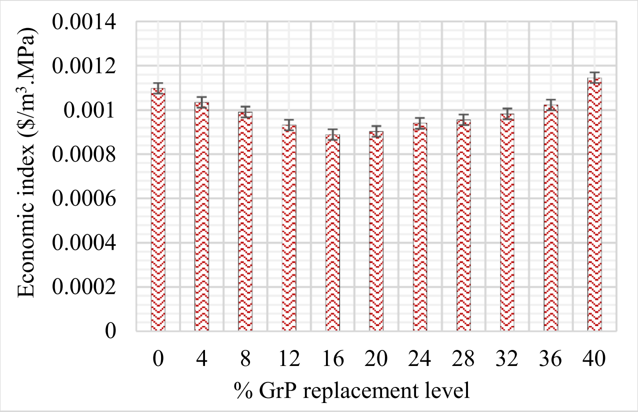

Fig. 19. EI of GrPBC mortar mixes.

This study reveals that environmental impacts could be attained by replacing recycled waste material (GrP) with conventional binder (OPC). Besides, it presents a plethora of opportunities for sustainability and economic effectiveness. The precise mix design quantity, source, and mode of delivery of product's constituents have a considerable impact on variability, as this study admits. The transportation and cradle-to-gate components of the cradle-to-site boundary can be further studied.

Funding

No funding was associated with this research.

CRediT authorship contribution statement

Vhishva laxmy: Visualization, Validation. **Jagadesh P:** Writing – original draft, Data curation, Conceptualization. **Supikshaa K:** Supervision, Project administration. **Sarulatha A:** Methodology, Investigation. **Hareesh Muthu A:** Resources, Formal analysis. **Solomon Oyebisi:** Writing – review & editing.

Declaration of Competing Interest

The authors declare that they have no known competing financial interests or personal relationships that could have appeared to influence the work reported in this paper.

Data availability

Data will be made available on request.

Acknowledgments

The authors wish to thank the teaching and technical staff of the strength of materials laboratory and structural engineering laboratory for their support throughout the study's investigations.

References

[1] S. Marinković, M. Malešev, I. Ignjatović, Life cycle assessment (LCA) of concrete made using recycled concrete or natural aggregates. In Eco-Efficient Construction and Building Materials, Woodhead Publishing, Cambridge, 2014, pp. 239–266.
[2] P. Jagadesh, A. Ramachandramurthy, R. Murugesan, Processing of sugar cane bagasse ash and properties of processed sugar cane bagasse ash blended mortars", Sadhana Acad. Sci. 47 (2022) 187, https://doi.org/10.1007/s12046-022-01963-7.
[3] H. Changdi, M. Brijes, S. Qingwen, Z. Yun, L. Dajun, W. Xiao, Correlations between mineral composition and mechanical properties of granite using digital image processing and discrete element method", Int. J. Min. Sci. Technol. 33 (8) (2023) 949–962, https://doi.org/10.1016/j.ijmst.2023.06.003.

[4] WNSA, World granite production data by World Natural Stone Association (WNSA), 2014. ⟨http://www.wonasa.com/en/reports.html⟩.

[5] J. Lohar, N. Shrivastava, A. Sharma, Feasibility of granite processing waste as a fill material in geotechnical applications, Mater. Today Proc. (2023), https://doi.org/10.1016/j.matpr.2023.04.655.

[6] A. Elmoaty, M.A. Elmoaty, Mechanical properties and corrosion resistance of concrete modified with granite dust, Constr. Build. Mater. 47 (2013) 743–752, https://doi.org/10.1016/j.conbuildmat.2013.05.054.

[7] G. Rojo-Lopez, S. Nunes, B. Gonzalez-Fonteboa, A.F. Martinez, Quaternary blends of portland cement, metakaolin, biomass ash and granite powder for production of self-compacting concrete, J. Clean. Prod. 266 (2020) 121666, https://doi.org/10.1016/j.jclepro.2020.121666.

[8] X. Gao, B. Yuan, Q.L.L. Yu, H.J.H.J.H. Brouwers, Characterization and application of municipal solid waste incineration (MSWI) bottom ash and waste granite powder in alkali activated slag, J. Clean. Prod. 164 (2017) 410–419, https://doi.org/10.1016/j.jclepro.2017.06.218.

[9] M.T.B. Silva, B.S. Hermo, E. Garcia-Rodeja, N.V. Freire, Reutilization of granite powder as an amendment and fertilizer for acid soils, J. Chemosphere 61 (7) (2005) 993–1002, https://doi.org/10.1016/j.chemosphere.2005.03.010.

[10] S. Ghannam, H. Najm, R. Vasconez, Experimental study of concrete made with granite and iron powders as partial replacement of sand, Sustain. Mater. Technol. 9 (2016) 1–9, https://doi.org/10.1016/j.susmat.2016.06.001.

[11] F. Kala, Effect of granite powder on strength properties of concrete, Int. J. Eng. Sci. Res. Inventory 1 (12) (2013) 36–50.

[12] G. Sirianni, H.D. Hosgood, M.D. Slade, J. Borak, Particle size distribution and particle size-related crystalline silica content in granite quarry dust, J. Occup. Environ. Hyg. 5 (5) (2008) 279–285, https://doi.org/10.1080/15459620801947259.

[13] M. Vijayalakshmi, A.S.S. Sekar, G.G. Prabhu, Strength and durability properties of concrete made with granite industry waste, Constr. Build. Mater. 46 (2013) 1–7, https://doi.org/10.1016/j.conbuildmat.2013.04.018.

[14] S. Singh, S. Khan, R. Khandelwal, A. Chugh, R. Nagar, Performance of sustainable concrete containing granite cutting waste, J. Clean. Prod. 119 (2016) 86–98, https://doi.org/10.1016/j.jclepro.2016.02.008.

[15] S. Singh, R. Nagar, V. Agrawal, A Review on properties of sustainable concrete using granite dust as replacement for river sand, J. Clean. Prod. 126 (2016) 74–87, https://doi.org/10.1016/j.jclepro.2016.03.114.

[16] G. Prokopski, V. Marchuk, A. Huts, The effect of using granite dust as component of concrete mixture, Case Stud. Constr. Mater. 13 (2020) e00349, https://doi.org/10.1016/j.cscm.2020.e00349.

[17] H.E. Elyamany, A.E.M. Elmoaty, B. Mohamed, Effect of filler types on physical, mechanical and microstructure of self-compacting concrete and Flow-able concrete, Alexendria Eng. J. 53 (2014) 295–307, https://doi.org/10.1016/J.AEJ.2014.03.010.

[18] L.K. Gupta, A.K. Vyas, Impact on mechanical properties of cement sand mortar containing waste granite powder, Constr. Build. Mater. 191 (2018) 155–164, https://doi.org/10.1016/j.conbuildmat.2018.09.203.

[19] D.M. Sadek, M.M. El-Attar, H.A. Ali, Reusing of marble and granite powders in self-compacting concrete for sustainable development, J. Clean. Prod. 121 (2016) 19–32, https://doi.org/10.1016/j.jclepro.2016.02.044.

[20] Y. Li, H. Yu, L. Zheng, J. Wen, C. Wu, Y. Tan, Compressive strength of fly ash magnesium oxychloride cement containing granite wastes, Constr. Build. Mater. 38 (2013) 1–7, https://doi.org/10.1016/j.conbuildmat.2012.06.016.

[21] S.H. Chu, Effect of paste volume on fresh and hardened properties of concrete, Constr. Build. Mater. 218 (2019) 284–294, https://doi.org/10.1016/j.conbuildmat.2019.05.131.

[22] A. Chajec, The use of granite powder waste in cementitious composites, J. Mater. Res. Technol. 25 (2023) 4761–4783, https://doi.org/10.1016/j.jmrt.2023.06.253.

[23] Y. Briki, M. Zajac, M. Haha, Ben, K. Scrivener, Impact of limestone fineness on cement hydration at early age, Cem. Concr. Res. 147 (2021) 106515, https://doi.org/10.1016/j.cemconres.2021.106515.

[24] R. Kamegawa, M. Naito, K. Miyata, Functionalization of silica nanoparticles for nucleic acid delivery, Nano Res. 11 (2018) 5219–5239, https://doi.org/10.1007/S12274-018-2116-7.

[25] X. Lv, Y. Lin, X. Chen, Y. Shi, R. Liang, R. Wang, Z. Peng, Environmental impact, durability performance, and interfacial transition zone of iron ore tailings utilized as dam concrete aggregates, J. Clean. Prod. 292 (2021) 126068, https://doi.org/10.1016/j.jclepro.2021.126068.

[26] M. Dobiszewska, A.K. Schindler, W. Pichor, Mechanical properties and interfacial transition zone microstructure of concrete with waste basalt powder addition, Constr. Build. Mater. 177 (2018) 222–229, https://doi.org/10.1016/j.conbuildmat.2018.05.133.

[27] A. Karmegam, A. Kalidass, Reusing granite sawing waste in self-compacting concrete with polypropylene fiber at low-volume fractions, Struct. Concr. 20 (2) (2019) 766–773, https://doi.org/10.1002/suco.201800155.

[28] F.K. Thomas, P. Partheeban, Study on the effect of granite powder on concrete properties, Proc. Inst. Civ. Eng. Constr. Mater. 163 (2) (2010) 63–70, https://doi.org/10.1680/coma.2010.163.2.63.

[29] I. Taji, S. Ghorbani, J. de Brito, V.W.Y. Tam, S. Sharifi, A. Davoodi, M. Tavakkolizadeh, Application of statistical analysis to evaluate the corrosion resistance of steel rebars embedded in concrete with marble and granite waste dust, J. Clean. Prod. 210 (2019) 837–846, https://doi.org/10.1016/j.jclepro.2018.11.091.

[30] T. Ramos, A.M. Matos, B. Schmidt, J. Rio, J. Sousa-Coutinho, Granitic quarry sludge waste in mortar: effect on strength and durability, Constr. Build. Mater. 47 (2013) 1001–1009, https://doi.org/10.1016/j.conbuildmat.2013.05.098.

[31] E. Tsangouri, D.G. Aggelis, T. Matikas, A.C. Mpalaskas, Acoustic emission activity for characterizing fracture of marble under bending, Appl. Sci. 6 (1) (2015) 6, https://doi.org/10.3390/app6010006.

[32] A.C. Mpalaskas, T.E. Matikas, D. Van Hemelerijck, S. Iliopoulos, G.S. Papakitsos, D.G. Aggelis, "Acoustic signatures of different damage modes in plain and repaired granite specimens", Proc. SPIE 9439 (2015) 10. ⟨https://10.1117/12.2085040⟩.

[33] A.K. Thomoglou, J.G. Fantidis, M.E. Voutetaki, Z.S. Metaza, C.E. Chalioris, Mechanical characterization of nano-reinforced mortar: X-ra micro-CT for 3D imaging of microstructure, Eng. Proc. 41 (1) (2023) 4, https://doi.org/10.3390/engproc2023041004.

[34] A.K. Thomoglou, M.G. Falara, M.E. Voutetaki, J.G. Fantidis, B.A. Tayeh, C. E. Chalioris, Electromechanical properties of multi-reinforced self-sensing cement-based mortar with MWCNTs, CFs and PPs, Constr. Build. Mater. 400 (2023) 132566, https://doi.org/10.1016/j.conbuildmat.2023.132566.

[35] D.M. Nega, B.W. Yifru, W.Z. Taffese, Y.K. Ayele, M.D. Yehualaw, Impact of partial replacement of cement with blend of marble and granite waste powder on mortar", Appl. Sci. 13 (115) (2023) 8998, https://doi.org/10.3390/app13158998.

[36] K. Boakye, M. Khorami, Mechanical and durability performance of ternary blended calcined clay and pulverized granite mortar composites, Adv. Mater. Process. Technol. (2023), https://doi.org/10.1080/2374068X.2023.226459.

[37] A. Jain, R. Gupta, S. Chaudhary, Performance of self-compacting concrete comprising granite cutting waste as fine aggregate, Constr. Build. Mater. 221 (2019) 539–552, https://doi.org/10.1016/j.conbuildmat.2019.06.104.

[38] A.O. Mashaly, B.N. Shalaby, M.A. Rashwan, Performance of mortar and concrete incorporating granite sludge as cement replacement, Constr. Build. Mater. 169 (2018) 800–818, https://doi.org/10.1016/j.conbuildmat.2018.03.046.

[39] ISO, ISO 14040., "Environmental Management-Life cycle assessment-Principles and framework" (International Organization for Standardization), ISO, Geneva, Switzerland, 2006.

[40] CEC (2010). Europe 2020., "A strategy for smart, sustainable and inclusive growth", Communication from the Commission COM (2010) 2020 final.

[41] CEC, Roadmap to a resource efficient Europe, Commun. Comm. COM 2011 (2011) 571.

[42] CEC (2014)., Resources efficiency opportunities in the building sector, Communication from the Commission COM (2014) 445.

[43] UNEP (2004)., "Why take a life cycle approach? UNEP", Paris, p.28. Available at ⟨www.unep.fr/shared/publications/pdf/DTIx0585xPA-WhyLifeCycleEN.pd⟩.

[44] UNEP (2015)., UNEP-SETAC life cycle initiative, Website: ⟨http://www.lifecycleinitiative.org/⟩.

[45] S. Oyebisi, F. Olutoge, P. Kathirvel, I. Oyaotuderekumor, D. Lawanson, J. Nwani, A. Ede, R. Kaze, Sustainability assessment of geopolymer concrete synthesized by slag and corncob ash, Case Stud. Constr. Mater. 17 (2022) e01665, https://doi.org/10.1016/j.cscm.2022.e01665.

[46] S. Oyebisi, T. Aloymari, Cement-based concrete modified with Vitellaria paradoxa ash: a lifecycle assessment, Constr. Build. Mater. 342 (2022) 127906, https://doi.org/10.1016/j.conbuildmat.2022.127906.

[47] Indian Standard (IS) 12269, Ordinary Porland Cement, 53 grade – specifications, Bureau of Indian Standards, New Delhi, 2013.

[48] Indian Standard (IS) 1727, Methods of test for pozzolanic materials, Bureau of Indian Standards, New Delhi, 2004.

[49] Indian Standard IS 4031 (Part 2), Methods of physical tests for hydraulic cement. Part 2 – Determination of fineness, Bureau of Indian Standards, New Delhi, 2004.

[50] Indian Standard IS 4031 (Part 4), Methods of Physical Tests for Hydraulic Cement. Part 4 – Determination of Consistency of Standard Cement Paste, Bureau of Indian Standards, New Delhi, 2005.

[51] Indian Standard IS 5513, Victa Apparatus – Specifications, Bureau of Indian Standards, New Delhi, 2005.

[52] Indian Standard IS 4031 (Part 5), Methods of Physical Tests for Hydraulic Cement. Part 5 – Determination of Initial and Final Setting Times, Bureau of Indian Standards, New Delhi, 2005.

[53] Indian Standard IS 4031 (Part 6), Methods of Physical Tests for Hydraulic Cement. Part 6 – Determination of Compressive Strength of Hydraulic Cement Other than Masonry Cement, Bureau of Indian Standards, New Delhi, 2003.

[54] American Standard of Testing Method (ASTM C 311), Standard Test Methods for sampling and testing fly ash or natural pozzolans for use in Portland cement concrete, ASTM international, United States, 2007.

[55] Hammond, G.P., Jones, C., "Inventory of (embodied) Carbon & Energy Database (ICE)", Version 2.0 (Ed. F. Lowrie, and P. Tse), United Kingdom, 2011.

[56] S. Fernando, C. Gunasekara, D.W. Law, M.C.M. Nasvi, S. Setunge, R. Dissanayake, Life cycle assessment and cost analysis of fly ash–rice husk ash blended alkali-activated concrete, J. Environ. Manag. 295 (2020) 113140.

[57] P.L. Meena, J.K. Saini, A.K. Surela, Granite waste mediated synthesis of polyaniline nanofibers for the catalytic reduction of hazardous organic water toxins, Inorg. Chem. Commun. 152 (2023) 110688, https://doi.org/10.1016/j.inoche.2023.110688.

[58] B. Ngayakamo, A. Bello, A.P. Onwualu, Valorization of granite waste powder as a secondary flux material for sustainable production of ceramic tiles, Clean. Mater. 4 (2022) 100055, https://doi.org/10.1016/j.clema.2022.100055.

[59] C. Ramadji, A. Messan, E. Prud'Home, Influence of granite powder on phyisco-mechanical and durability properties of mortar, Materials 13 (23) (2020) 5406, https://doi.org/10.3390/ma13235406.

[60] M.E. Tawfik, S.B. Eskander, N.M. Ahmed, Potential applications of granite waste powder as an add-value polymer composite product, Polym. Polym. Compos. 23 (2022), https://doi.org/10.1177/09673911221110138.

[61] Z. Liu, C. Wang, M. Zhang, J. ShaoCracking property and brittleness evaluation of granite under high-temperature true triaxial compression in geothermal systems", Geo-mechanic Geo-physics Geo-energy Geo-resources., 9(99):1-23, 2023. https://doi.org/10.1007/s40948-023-00631-2.

[62] I.L. Boadella, F.L. Gayarre, J.S. González, J.M. Gomez-Soberon, C.L. Perez, M. S. Lopez, J. Brito, The influence of granite cutting waste on the properties of ultra-high-performance concrete, Materials 12 (4) (2019) 634–647, https://doi.org/10.3390/ma12040634.

[63] E.A. Shamsabadi, M. Ghalehnovi, J. Brito, A. Khodabakhshian, Performance of concrete with waste granite powder: Effects of superplasticizers, Appl. Sci. 8 (10) (2018) 1808–1828, https://doi.org/10.3390/app8101808.

[64] C.M. Abreu, A. Covelo, B. Diaz, L. Freire, X.R. Novoa, M.C. Perez, Electrochemical behaviour of iron in chlorinated alkaline media. The effect of slurries from granite processing, J. Braz. Chem. Soc. 18 (6) (2007) 1158–1163.

[65] B. Barra, L. Momm, Y. Guerrero, L. Bernucci, Characterization of granite and lime stone powders for use as fillers in bituminous mastics dosage, Ann. Braz. Acad. Sci. 86 (2) (2014) 995–1002, https://doi.org/10.1590/0001-3765201420130165.

[66] K.G. Reddy, K. Yarakkula, Exploration of geo-mineral compounds in granite mining soils using XRD pattern data analysis, IOP Conf. Ser. Mater. Sci. Eng. 263 (2017) 032003, https://doi.org/10.1088/1757-899X/263/3/032003.

[67] N. Sapiai, A. Jumahat, M. Jawaid, M.Z. Abu, M. Chalid, Mechanical performance of granite fine fly dust filled basalt/glass polyurethane polymer hybrid composites, *Polymer* 13 (18) (2021) 3032, https://doi.org/10.3390/polym13183032.

[68] A. Chajec, Granite powder vs. fly ash for the sustainable production of air-cured cementitious mortars, Materials 14 (5) (2021) 1208, https://doi.org/10.3390/ma14051208.

[69] A. Amani, A. Babazadeh, A. Sabohanian, A. Khalilianpoor, Mechanical properties of concrete pavements containing combinations of waste marble and granite powders, Int. J. Pavement Eng. (2019), https://doi.org/10.1080/10298436.2019.1702662.

[70] A. Remoroza, B. Moghtaderi, E. Doroodchi, Fluid rock interaction under reservoir conditions pertinent to hot dry rock engineered geothermal systems, Melbourne, Australia, 19-25 April, Proc. World Geotherm. Congr. 2015 (2015). Melbourne, Australia, 19-25 April.

[71] A. Stempkowska, T. Gawenda, A. Chajec, Ł. Sadowski, Effect of granite powder grain size and grinding time of the properties of cementitious composites, Materials *15* (2022) 8837, https://doi.org/10.3390/ma15248837.

[72] J. Kouam, V. Songmene, A. Bahloul, A.M. Samuel, Characterization of Si and SiO_2 in dust emitted during granite polishing as a function of cutting conditions, Materials 15 (2022) 3965, https://doi.org/10.3390/ma15113965.

[73] Y. Yin, H. Yin, Z. Wu, C. Qi, H. Tian, W. Zhang, Z. Hu, L. Feng, Characterization of coals and coal ashes with high Si content using combined second – derivative infrared spectroscopy and Raman spectroscopy, Crystals 9 (10) (2019) 513, https://doi.org/10.3390/cryst9100513.

[74] A. Guedes, Characterization of fly ash from power plant and surroundings by micro-Raman spectroscopy, Int. J. Coal Geol. 73 (3-4) (2008) 359–370, https://doi.org/10.1016/j.coal.2007.09.001.

[75] M.A. El-Sherbiny, G.A. El-Chaghaby, El-Shafea, Treatment of aquaculture waste effluent to be reused in fish culture in Egypt, Egypt. J. Aquat. Biol. Fish. 23 (1) (2019) 233–243, https://doi.org/10.21608/ejabf.2019.27272.

[76] R.K.S. Garigipati, R. Malkapuram, Characterization of novel composites from polybenzoxazine and granite powder, SN Appl. Sci. 2 (2020) 1545, https://doi.org/10.1007/s42452-020-03333-6.

[77] S.B. Eskander, T.A. Bayoumi, M.E. Tawfik, H. Mansour, Newly developed cement-ground granite scraps composite for solidification/stabilization of radioactive wastes: characterization and evaluation of the mechanical durability, Polym. Bull. 80 (2023) 6635–6655, https://doi.org/10.1007/s00289-022-04350-8.

[78] S.C. Paul, M.Y. Miah, A. Gafur, R.C. Das, Study of thermal properties of granite powder (scrap) reinforced polyester resin composite, J. Adv. Chem. Eng. vol.7 (2017) 159, https://doi.org/10.4172/2090-4568.1000159.

[79] M. Pan, X. Li, X. Wu, F. Zhao, C. Ma, Preparation of thermal insulation materials based on granite waste using a high-temperature micro-foaming method, J. Asian Ceram. Soc. Vol.10 (No.1) (2022) 223–229, https://doi.org/10.1080/21870764.2022.2034713.

[80] E. Plevova, L. Vaculikova, A. Kozusnikova, M. Ritz, S.G. Martynkova, Thermal expansion behavior of granites", J. Therm. Anal. Calor. Vol.123 (2016) 1555–1561, https://doi.org/10.1007/S10973-015-4996-z.

[81] C.M.F. Vieira, S.N. Monteiro, Characterization of granite waste for incorporation in red ceramic, Mater. Sci. Forum Vol.498-499 (2005) 728–733, https://doi.org/10.4028/www.scientific.net/MSF.498-499.728.

[82] ASTM Standard C618-12a, Standard Specification for Coal Fly Ash and Raw or Calcined Natural Pozzolan for Use in Concrete, ASTM International, USA, 2014.

[83] K. Jayachandran, R. Pillai, Statistical distributions for the corrosion rates of conventional and prestressing steel reinforcement embedded in chloride contaminated mortar, Corrosion 73 (9) (2017) 1119–1131, https://doi.org/10.5006/2330.

[84] S.S.S.A. Nedunuri, S.G. Serstse, S. Muhammad, Microstructural study of Portland cement partially replaced with fly ash, ground granulated blast furnace slag and silica fume as determined by pozzolanic activity, Constr. Build. Mater. 238 (2020) 117561, https://doi.org/10.1016/j.conbuildmat.2019.117561.

[85] K. Chintalapudi, R.M.R. Pannem, Enhanced chemical resistance to sulphuric acid attack by reinforcing graphene oxide in ordinary and Portland pozzolana cement mortars", Case Stud. Constr. Mater. 17 (2022) e01452 https://doi.org/10.1016/j.cscm.2022e01452.

[86] P. Jagadesh, T. Karthik Prabhu, M. Charai, I.Y. Hakeem, E. Madenci, Y.O. Ozkilic, "A potential review on the influence of nanomaterials on the mechanical properties of high strength concrete, Steel Compos. Struct. 48 (6) (2023) 649–666, https://doi.org/10.12989/scs.2023.48.6.649.

[87] E. Serelis, V. Vaitkevicius, Z. Rudzionis, V. Kersevicius, Waste of granite dust utilization in ultra-light weight concrete, IOP Conf. Ser. Mater. Sci. Eng. vol.442 (2018) 012004, https://doi.org/10.1088/1757-899X/442/1/012004.

[88] S.B. Singh, P. Munjal, N. Thammishetti, Role of water/cement ratio on strenght development of cement mortar, J. Build. Eng. 4 (2015) 94–100, https://doi.org/10.1016/j.jobe.2015.09.003.

[89] V. Vanathi, V. Nagarajan, P. Jagadesh, Influence of sugarcane bagasse ash on mechanical properties of geopolymer concrete, J. Build. Eng. 79 (2023) 107836, https://doi.org/10.1016/j.jobe.2023.107836.

[90] M.A.O. Mydin, P. Jagadesh, A. Bahrami, A. Dulaimi, Y.O. Ozkilic, M.M.A. B. Abdullah, R.P. Jaya, Use of calcium carbonate nanoparticles in production of nano-engineered foamed concrete, J. Mater. Res. Technol. 26 (2023) 4405–4422, https://doi.org/10.1016/j.jmrt.2023.08.106.

[91] D.A. Adesanya, A.A. Raheem, Development of corn cob ash blended cement, Constr. Build. Mater. 23 (2009) 347–352, https://doi.org/10.1016/j.conbuildmat.2007.11.013.

[92] A.A. Raheem, A.I. Ige, Chemical composition and physico-mechanical characteristics of saw dust ash blended cement, J. Build. Eng. 21 (2019) 404–408, https://doi.org/10.1016/j.jobe.2018.10.014.

[93] Y. Knop, A. Peled, Sustainable blended cements – influences of packing density on cement paste chemical efficiency, Materials 11 (4) (2018) 625, https://doi.org/10.3390/ma11040625.

[94] S. Afroz, Y. Zhang, Q.D. Nguyen, T. Kim, A. Castel, Shrinkage of blended cement concrete with fly ash or limestone calcined clay, Mater. Struct. 56 (2023) 15, https://doi.org/10.1617/s11527-023-02099-8.

[95] K.L. Scrivener, A.K. Crumbie, P. Laugesen, The interfacial transition zone (ITZ) between cement paste and aggregate in concrete, Interface Sci. Vol.12 (2004) 411–421.

[96] J. Wang, C. Xue, Y. Zhang, Q. Li, Y. Han, H. Qiao, Study of early-age hydration, mechanical properties development, and microstructure evolution of manufactured sand concrete mixed with granite stone powder, Materials 16 (2023) 4857, https://doi.org/10.3390/ma16134857.

[97] Z.Z. Wozniak, A. Chajec, L. Sadowski, Effect of the partial replacement of cement with waste granite powder on the properties of fresh and hardened mortars for masonry applications, Materials 15 (24) (2022) 9066, https://doi.org/10.3390/ma15249066.

[98] A.B. Kizilkanat, D. Oktay, N. Kabay, M.M. Tufekci, Comparative experimental study of mortars incorporating pumice powder or fly ash, J. Mater. Civ. Eng. 28 (2) (2015) 04015119, https://doi.org/10.10161/(ASCE)MT.1943-5533.0001407.

[99] M.J. Mwiti, T.J. Karanja, W.J. Muthengia, Properties of activated blended cement containing high content of calcined clay, Heliyon 4 (8) (2018) e00742, https://doi.org/10.1016/j.heliyon.2018.e00742.

[100] J. Liu, J. Li, J. Ye, F. He, Setting behaviour, mechanical property and biocompatibility of anti-washout wollastonite/calcium phosphate composite cement", Ceram. Int. 42 (12) (2016) 13670–13681, https://doi.org/10.1016/j.ceramint.2016.05.165.

[101] Y.L. Yaphary, Z. Yu, R.H.W. Lam, D. Lau, Effect of triethanolamine on cement hydration toward initial setting time, Constr. Build. Mater. 141 (2017) 94–103, https://doi.org/10.1016/j.conbuildmat.2017.02.072.

[102] N. Dave, A.K. Misra, A. Srivastava, S.J. Kaushik, Setting time and standard consistency of quaternary binders: the influence of cementitious material addition and mixing, Int. J. Sustain. Built Environ. 6 (1) (2017) 30–36, https://doi.org/10.1016/j.ijsbe.2016.10.004.

[103] S. Hollanders, R. Adriaens, J. Skibsted, O. Cizer, J. Elsen, Pozzolanic reactivity of pure calcined clays, Appl. Clay Sci. 132-133 (2016) 552–560, https://doi.org/10.1016/j.clay.2016.08.003.

[104] M.C.G. Juenger, R. Siddique, Recent advances in understanding the role of supplementary cementitious materials in concrete, Cem. Concr. Res. 78 (2015) 71–80, https://doi.org/10.1016/j.cemconres.2015.03.018.

[105] G. Medina, I.F. Sáez del Bosque, M. Frías, M.I. Sánchez de Rojas, C. Medina, Granite quarry waste as a future eco-efficient supplementary cementitious material (SCM): Scientific and technical considerations, J. Clean. Prod. 148 (2017) 467–476, https://doi.org/10.1016/j.jclepro.2017.02.048.

[106] P. Jagadesh, A. Ramachandramurthy, P. Rajasulochana, M.A. Hasan, R. Murugesan, A.H. Khan, H.M. Magbool, N.A. Khan, Effect of processed sugarcane bagasse ash on compressive strength of blended mortar and assessments using statistical modelling", Case Stud. Constr. Mater. 19 (2023) e02435 https://doi.org/10.1016/jj.cscm.2023.e02435.

[107] H.F. Isleem, P. Jagadesh, J. Ahmad, S. Qaidi, F. Althoey, H.M. Najm, "Finite element and analytical modelling of PVC confined concrete columns under axial compression", Front. Mater. 9 (2022) https://doi.org/10.3389/fmats.2022.1011675.

[108] P. Jagadesh, J. Prado-Gil, N. Silva-Monteiro, R. Martinez-Garcia, Assessing the compressive strength of self-compacting concrete with recycled aggregates from mix ratio using machine learning approach, J. Mater. Res. Technol. 24 (2023) 1483–1498, https://doi.org/10.1016/j.jmrt.2023.03.037.

[109] P. Jagadesh, A. Ramachandramurthy, R. Murugesan, T. Karthik Prabhu, Adaptability of sugar cane bagasse ash in mortar, J. Inst. Eng. India Ser. A 100 (2) (2019) 225–240, https://doi.org/10.1007/s40030-019-00359-x.

[110] B. Siva, R. Paradelo, N. Vazquez, E. Garcia-Rodeja, M.T. Barral, Effect of the addition of granite powder to an acidic soil from Galicia (NW Spain) in comparison with lime", Environ. Earth Sci. 68 (2013) 429–437, https://doi.org/10.1007/s12665-012-1747-3.

[111] A. ElNemr, Generating water/binder ratio to strength curves for cement mortar used in masnory walls, Constr. Build. Mater. 233 (2020) 117249, https://doi.org/10.1016/j.conbuildmat.2019.117249.

[112] G.A. Rao, Role of water binder ratio on the strength development in mortars incorporated with silica fume, Cem. Concr. Res. 31 (2001) 443–447.

[113] Abrams Duff, Design of concrete mixtures. Bulletin No.1, Structural Materials Laboratory, Lewis Institute, Chicago, 1918, p. 20.

[114] Feret, R. (1892). Surlacompacité des mortiers hydrauliques. ⟨⟨http://www.bcin.ca/Interface/openbcin.cgi?Submit=submit&Chinkey=123645⟩⟩ (Accessed 20 August 2023).

[115] J. Bolomey, Détermination de la résistance à la compression des mortiers et bétons, Bull. Tech. La Suisse Rom. 51 (1925), https://doi.org/10.5169/seals-39510.

[116] A. Goldman, A. Bentur, The influence of micro fillers on enhancement of concrete strength, Cem. Concr. Res. 23 (4) (1993) 962–972. DOI: 10.1016/0008-8846(93)90050-J.

[117] A. Abubakar, A. Mohammed, D. Samson, Assessment of embodied energy and CO_2 emission of concrete containing corncob ash, Int. J. Sustain. Green. Energy 10 (2) (2021) 76–84. ⟨http://www.sciencepublishinggroup.com/j/ijsge⟩.

[118] N. Lovecchio, F. Shaikh, M. Rosano, R. Ceravolo, W. Biswas, Environmental assessment of supplementary cementitious materials and engineered nanomaterials concrete, AIMS Environ. Sci. 7 (1) (2020) 13–30, https://doi.org/10.3934/environsci.2020002.

[119] R. Robayo-Salazar, J. Mejía-Arcila, R.M. De Gutierrez, E. Martínez, Life cycle assessment (LCA) of an alkali-activated binary concrete based on natural volcanic pozzolan: a comparative analysis to OPC concrete, Constr. Build. Mater. 176 (2018) 103–111, https://doi.org/10.1016/j.conbuildmat.2018.05.017.

[120] A. Sagheb, E. Vafaeihosseini, R.P. Kumar, The role of building construction materials on global warming lessons for architects, Natl. Conf. Recent Trends Civ. Mech. Eng. (2011).

[121] K.M. Rahla, R. Mateus, L. Braganca, Comparative sustainability assessment of binary blended concrete using Supplementary Cementitious Materials (SCMs) and Ordinary Portland Cement (OPC), J. Clean. Prod. 220 (2019) 445–459, https://doi.org/10.1016/j.jclepro.2019.02.010.

[122] L. Braganca, R. Mateus, H. Koukkari, Building sustainability assessment, *Sustain*ability 2 (7) (2010) 2010–2023, https://doi.org/10.3390/su2072010.

[123] R. Bajpai, K. Choudhary, A. Srivastava, K.S. Sangwan, M. Singh, Environmental impact assessment of fly ash and silica fume based geopolymer concrete, J. Clean. Prod. 254 (2020) 120147, https://doi.org/10.1016/j.jclepro.2020.120147.